Pergamon

Geochimica et Cosmochimica Acta, Vol. 67, No. 3, pp. 487–505, 2003

0016-7037/03 $22.00 + .00

PII S0016-7037(02)01089-X

"Reactive" harzburgites from Huinan, NE China: Products of the lithosphere-asthenosphere interaction during lithospheric thinning?

YI-GANG XU,[1,*] MARTIN A. MENZIES,[2] MATTHEW F. THIRLWALL,[2] XIAO-LONG HUANG,[1] YING LIU,[1] and XIAO-MING CHEN[3]

[1]Guangzhou Institute of Geochemistry, Chinese Academy of Sciences, 510640 Guangzhou, China
[2]Geology Department, Royal Holloway University of London, TW20 OEX Egham Surrey, UK
[3]State Key Laboratory for Mineral Deposit Research, Department of Earth Sciences, Nanjing University, Nanjing, China

(*Received February* 4, 2002; *accepted in revised form July* 25, 2002)

Abstract—Petrologic, trace element and Sr-Nd isotopic studies of mantle xenoliths in Quaternary basalts from Huinan, NE China provide constraints on the origin of coarse-grained harzburgites and the nature of lithosphere-asthenosphere interaction during lithospheric thinning. The Huinan harzburgites have a secondary recrystallized texture and their composition deviates from the partial melting trend of residual peridotites. The convex-upward REE pattern and a positive Cr-Yb correlation in clinopyroxene imply an interaction with basaltic melts at a high melt/rock ratio. The Huinan harzburgites are therefore not simple residues of partial melting, but likely resulted from melt-rock interaction during which the percolating melts preferentially dissolved pyroxenes by precipitation of olivine, transforming lherzolite to harzburgite. The melt percolation-reaction enhanced grain boundary diffusion kinetics, and gave rise to the characteristic texture of these mantle rocks. These "reactive" harzburgites were eventually metasomatized by compositionally distinct small volume volatile-rich melts, which may be derived from the main harzburgite-forming event as a result of melt-consuming reaction. Most likely the formation of the Huinan harzburgites was coeval with thermo-tectonic erosion of the continental lithosphere by upwelling asthenospheric melts. Thermometric considerations suggest a relatively long time interval between lithospheric thinning and eruption of the host basalts, consistent with the contention that lithospheric thinning in eastern China may have peaked in the late Cretaceous. *Copyright © 2003 Elsevier Science Ltd*

1. INTRODUCTION

Harzburgite, an important rock type in the upper mantle, is traditionally interpreted as a residue of high degree partial melting of a fertile mantle source. Compared with coexisting lherzolites, harzburgites commonly show a higher degree of enrichment of highly incompatible elements (Frey and Green, 1974; McDonough and Frey, 1989; Xu et al., 1998b). This preferential LREE-enrichment in harzburgites has been explained by a number of hypotheses involving, (1) an enhanced permeability of harzburgites relative to lherzolites because of their olivine-rich character (Toramaru and Fujii, 1986); (2) a higher sensitivity of clinopyroxene-poor peridotite whole-rock compositions to enriched micro-inclusion trapped in minerals; and (3) a higher velocity of chromatographic fronts of incompatible elements in refractory peridotites (e.g., Bedini et al., 1997). In classic two-stage petrogenetic models (e.g., Frey and Green, 1974), melt extraction is linked to the modal composition and major element chemistry of such rocks and melt transfer is believed to be the source of the incompatible element concentrations. That is, the metasomatism only introduced incompatible elements in harzburgites without leaving any mineralogical imprint. However, Kelemen et al. (1992) found that many harzburgites are orthopyroxene-rich compared to normal partial melting residues. On this basis they suggested that harzburgites may result from interaction between a protolith and melts (i.e., "reactive" harzburgite). During this reaction, percolating melt preferentially dissolved clinopyroxene (cpx) and precipitated olivine (ol) and orthopyroxene (opx), transforming the lherzolite (cpx-bearing) to harzburgite (cpx-poor). The differences between "residual" and "reactive" harzburgites are not always clear and necessitate a comprehensive investigation of the mineralogy, texture and geochemistry.

Secondary recrystallized texture (Mercier and Nicolas 1975) requires coarse-grained silicate minerals (>5mm) in peridotites and this texture differs from protogranular textures by the presence of spinel disseminated along grain boundaries. Similar textures are widespread in the xenoliths from southern Massif Central, France (Lenoir et al., 2000) and are also observed in the Ronda massif (as "coarse-granular" peridotites, Van der Wal and Bodinier, 1996; Lenoir et al., 2001). The poikiloblastic type described at Boree, Massif Central (Berger. 1978; Xu et al., 1998a) may represent an extreme of the variation of secondary recrystallized textures. Secondary recrystallized texture has been previously interpreted as equigranular, modified by annealing and grain growth (Mercier and Nicolas, 1975). However, recent geochemical studies suggest that the development of this texture is associated with chemical modification rather than being an isochemical process (Downes et al., 1992; Van der Wal and Bodinier, 1996; Xu et al., 1998a; Lenoir et al., 2001). Despite the potential of a secondary texture as a diagnostic indicator of melt percolation, samples with this texture have not been systematically investigated and their geodynamic significance remains poorly understood.

The Quaternary volcanic cones in Huinan, northeastern China contain abundant harzburgite xenoliths that have a secondary recrystallized texture. This provides a good opportunity to decipher the nature of processes that were responsible for the textural development and generation of harzburgites, and the

* Author to whom correspondence should be addressed (yigangxu@gig.ac.cn).

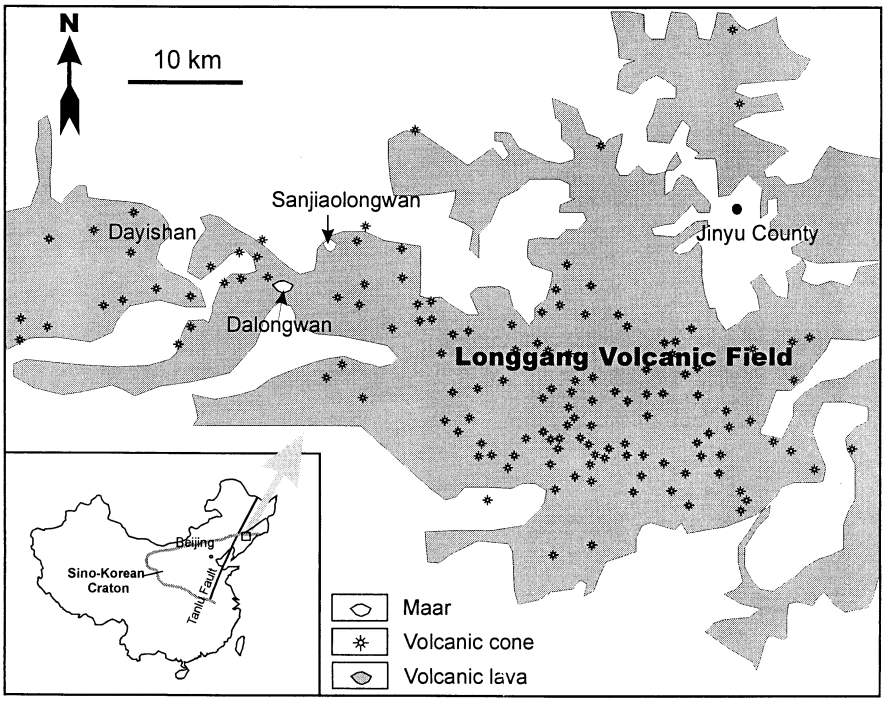

Fig. 1. Simplified geological map showing the distribution of volcanic cones in the Longgang area. The Longgang volcanic field is located in the northeast part of the Sino-Korean Craton.

factors controlling their petrogenesis. In this paper, we present new major and trace element and Sr-Nd isotopic data for peridotite xenoliths from Huinan. In terms of texture and equilibrium temperature, the Huinan harzburgites are comparable to the coarse-granular xenoliths from southern Massif Central (Lenoir et al., 2000). On the other hand, they resemble the Boree poikiloblastic xenoliths (Xu et al., 1998a) with regard to mineralogy and geochemistry (i.e., convex-upward REE pattern in cpx). The Huinan harzburgites also show some similarities with the coarse-granular peridotites from the Ronda massif in terms of texture and mineralogy (Van der Wal and Bodinier, 1996; Lenoir et al., 2001). Inspired from the previous studies on the Boree and Ronda peridotites, the role of melt percolation reactions is emphasized in the petrogenesis of the Huinan harzburgites. It is proposed that the Huinan harzburgites may represent the products of interaction of continental lithosphere, thinned by extension, with silicate melts from the asthenosphere.

2. SAMPLE DESCRIPTION AND PETROGRAPHY

The Longgang volcanic field in Jilin Province is located in the northeast part of the Sino-Korean Craton (see inset of Fig. 1). It covers an area of ~2000 km^2 and is composed of more than one hundred cinder cones (Fig. 1). Many of them were erupted in the early Pleistocene (0.6 Ma) (Fan et al., 2000a). Volcanic cones are composed of lavas and various pyroclastic deposits such as bombs, blocks, cinders and ash. The volcanism in this region was largely associated with activation and development of the northern part of the Tan-Lu and the Fushun-Mishan faults (Liu et al., 1992). Geophysical data indicate that the lithosphere in this rift zone is relatively thin (ca., 60 to 80 km) believed to be the result of extension and mantle upwelling (Chen et al., 1991).

Samples studied in this paper were collected from three volcanic maars, named Sanjiaolongwan (SJXO), Dalongwan (DLW) and Dayishan (DYS) ["Longwan" = "maar" in Chinese]. The xenoliths are large and very fresh with a maximum diameter of over 60 cm. They are spinel facies peridotites (i.e., depth <80 km) ranging from cpx-rich lherzolites to harzburgites. It is noted that the xenolith population varies considerably between different volcanic cones. For example, lherzolites are mainly from Sanjiaolongwan, whereas harzburgites are from Dalongwan and Dayishan. While no hydrous phases (e.g., amphibole and phlogopite) have been found in these xenoliths, there is an apparent correlation between modal composition and microstructure. Most lherzolites are similar to Group I peridotites (Frey and Prinz, 1978) with protogranular, porphyroclastic to equigranular textures (Mercier and Nicolas, 1975). Among the lherzolites, samples with porphyroclastic texture are the most abundant. Exsolution lamellae are present in some large opx porphyroclasts.

The harzburgites contain 61.7 to 81.2% ol, 13.6 to 32.1% opx, 2.7 to 5.7% cpx and 1 to 2.7% spinel (sp) (Table 2). They are characterized by a coarse grain-size with a diameter of olivine up to 8 mm and a dispersed distribution of pyroxene and spinel (Fig. 2a). Large olivines (>4 mm) are kinked and show curvilinear or irregular grain boundaries. Some of them contain small inclusions of sp (0.1 to 0.2 mm). In addition to small inclusions in olivines, spinels also occur as disseminated and interstitial phases at grain boundaries of silicates (Fig. 2a). The distribution of pyroxenes is extremely inhomogeneous in some harzburgites. Grain size of opx varies between 1 and 6 mm.

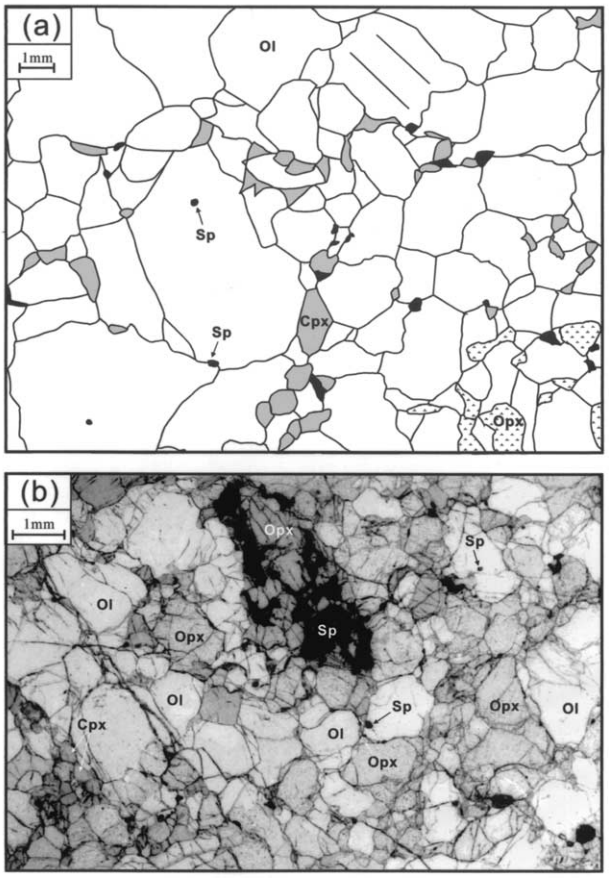

Fig. 2. Textural variation of the harzburgites from Huinan. (a) Line drawing of the thin section DYS-1 shows a large grain-size of olivines and a dispersed distribution of spinel and pyroxenes. The opx proportion in this thin section is significantly less than that estimated from whole rock and mineral chemistries, reflecting an inhomogeneous distribution of this mineral in the Huinan harzburgites. (b) Microphotography illustrates the coexistence of a dispersed distribution of pyroxene and spinel (lower part) and a pyroxene-spinel cluster (middle upper part) in sample DYS-7. This texture is considered as transitional between secondary recrystallized and protogranular ones.

Some opx are irregular in form and partially enclose olivines. No exsolution phenomenon is observed in harzburgite opx. Cpx are smaller in grain size (<0.5 mm) than ol and opx. They are generally interstitial along the grain boundaries and/or triple junction of other phases. Most cpx are generally green and clean but some (e.g., DLW-5) display a spongy appearance. This texture can be termed as secondary recrystallized according to the nomenclature of Mercier and Nicolas (1975). Similar texture (described as "coarse granular") has been documented in basalt-borne peridotite xenoliths from the southern Massif Central (Lenoir et al., 2000) and in the Ronda massif (Van der Wal and Bodinier, 1996). The Boree harzburgites are secondary in texture in *sense strict* of the nomenclature of Mercier and Nicolas (1975), although they contain extremely large olivine grains (commonly > 1 cm). As the Huinan harzburgites resemble the Boree xenoliths in terms of mineralogy and geochemistry (see next sections), it is conceivable that the secondarily recrystallized texture might have a range of petrographic features, with the poikiloblastic texture observed at Boree representing an extreme.

Some harzburgite samples show a texture transitional between secondary recrystallized and protogranular ones in terms of spinel and pyroxene relationships. This can be seen from Figure 2b, which shows coexistence of a dispersed distribution of pyroxene and spinel and a pyroxene-spinel cluster. A similar transitional texture has been observed in the poikiloblastic harzburgites from Boree which may have resulted from melt-rock reaction at expense of lherzolites (Xu et al., 1998a). As will be shown in the following sections, there is no difference in the mineralogy and geochemistry at the samples with this transitional texture and those with a typical secondary recrystallized texture. The pyroxene-spinel cluster is thus interpreted as a relict texture of the protolith. In this sense, the transitional texture may thus be taken as evidence for a genetic relationship between harzburgites and lherzolites.

3. SAMPLE PREPARATION AND ANALYTICAL METHODS

The xenoliths were sawn into slabs and the central parts were used for bulk-rock analyses and for mineral separation. The rocks were crushed in a steel mortar and ground in a carbide mill. Mineral separates were hand-picked under a binocular microscope. The minerals were analysed for major elements with a Joel Superprobe at Nanjing University. The bulk major element composition of 30 xenoliths was obtained using conventional wet chemical methods at Guangzhou Institute of Geochemistry, Chinese Academy of Sciences. The rocks, and a subset of clinopyroxene separates were analyzed for 25 trace elements including rare earth elements (REE) using an Inductively Coupled Plasma-Mass Spectrometer (ICP-MS) at the same institute. The mineral separates were leached with dilute HCl on a hot plate for 45 min before dissolution in a mixture of HF and HNO_3. The analytical procedure followed that described by Xu (2002). Precision for REE and other incompatible elements is estimated to be 5% from the international USGS reference samples BIR-1 and an internal standard (ROA-1). Measured values of standards are generally in good agreement with reference data (Xu, 2002). Duplicate runs gave <10% RSD (relative standard deviation) for most elements analyzed. Cpx separates of 19 samples were analysed for Sr-Nd isotopic composition at the University of London Isotope Laboratory at Royal Holloway using published experimental procedures (Thirlwall, 1991). Analyses of standards during the period of analysis were as follows: SRM987 gave $^{87}Sr/^{86}Sr$ = 710245 ± 14 (2S.D., n = 160); the in-house laboratory Nd standard (low Aldrich) gave $^{143}Nd/^{144}Nd$ = 0.511413 ± 7 (2S.D., n = 37).

4. RESULTS

4.1. Mineral Composition and Equilibrium Temperatures

The olivines in the Huinan lherzolites show a wide range in Mg/(Mg+Fe) ratio (Mg#, 0.88 to 0.916, mostly between 0.895 to 0.910). A relatively restricted Mg# (0.906 to 0.915) is noted for the harzburgites. No marked difference in minor elements (e.g., CaO, MnO and NiO) is noted for the olivines from the two rock types. Cpx in lherzolites have a narrow range in Mg# (0.90 to 0.918) compared to those in harzburgites (0.88 to 0.93). The harzburgite cpx have significantly higher Cr and comparable Na_2O and TiO_2 contents relative to those in lherzolites (Fig. 3a; Table 1).

Contrasting compositions are also noted for spinels in the Huinan lherzolites and harzburgites. The lherzolite spinels are comparable to those in Group I peridotites and most samples plot at the "primitive" end of the oceanic trend (Dick and

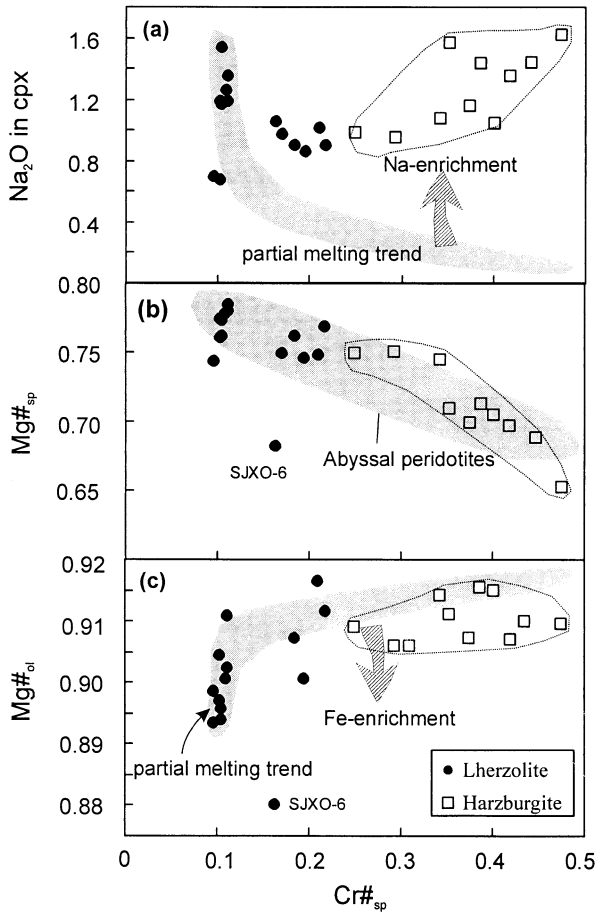

Fig. 3. Diagram illustrating concentration of selected elements in different minerals from peridotites from Huinan (Symbols: circles = lherzolites; squares = harzburgite). (a) Na_2O content in clinopyroxene. (b) $Mg\#_{sp}$ against $Cr\#_{sp}$ and (c) Correlation of Mg# of olivine versus Cr# of spinel. The progressive partial melting trend is from Xu et al., 1998a. The abyssal peridotite trend is after Dick and Bullen (1984). Note the Fe and Na enrichment in harzburgites and some lherzolites.

Bullen, 1984). The harzburgite spinels are characterized by higher Cr contents ($Cr\#_{sp}$) (Fig. 3b; Table 1). The TiO_2 contents in lherzolite spinels (except for the Fe-rich SJXO-6) are generally lower than in the harzburgite spinels (Table 1). In a plot of $Mg\#_{ol}$ against $Cr\#_{sp}$, most lherzolites follow the partial melting trend but some samples (e.g., SJXO-6) show significantly lower $Mg\#_{ol}$ at given $Cr\#_{sp}$, pointing to a Fe-enrichment in these samples (Xu et al., 1998a). Refertilization is also evident in harzburgites as they tend to plot below the partial melting trend (Fig. 3c).

Temperatures were estimated using the Ca-solubility in opx thermometer of Brey and Kohler (1990) and the Cr/Al-solubility in opx thermometer of Witt-Eickschen and Seck (1991). For a given sample, the Ca-in-opx thermometer gives slightly higher temperatures than the Cr-Al opx thermometer. The temperature estimates (based on the Ca-in-opx thermometer) for the Huinan lherzolites range between 850 to 1050 °C. A similar range is noted for the harzburgites (860 to 1060 °C).

4.2. Whole Rock Chemistry

Whole rock element abundances are given in Table 2 and illustrated in Figure 4. Al_2O_3, CaO and Yb contents in the Huinan lherzolites correlate negatively with MgO. The most fertile lherzolite samples (e.g., SJXO-1) are compositionally similar to the primitive mantle (PM, Jagoutz et al., 1979; Hart and Zindler, 1986). These trends, similar to those observed for xenoliths from Wangqing and other worldwide occurrences, are interpreted as residues of variable degrees of partial melting (Frey et al., 1985; Xu et al., 1998b; Takazawa et al., 2000). In contrast, the harzburgites deviate to some degree from the partial melting trend, due to slightly higher Al_2O_3 and CaO at comparable MgO (Fig. 4). The deviation from the common depletion trend becomes more significant for FeO and Na_2O and other incompatible elements (e.g., Ti, Zr, La, Yb; Fig. 4). Compatible elements (Cr, Ni) in the harzburgites show trends that are not coherent with that defined by the lherzolites (Fig. 4). Specifically, at comparable MgO, the Huinan harzburgites have relatively low Cr and Ni concentrations compared to theoretical harzburgites produced by partial melting and melt extraction.

The Huinan peridotites exhibit substantial variations in both absolute concentration of trace elements and chondrite-normalized REE patterns (Table 2, Fig. 5a). The fertile lherzolites show a LREE-depleted pattern with $(La/Yb)_n$ varying from 0.5 to 0.8 and Yb_n from 1.5 to 2.5. In PM-normalized spidergram, weak negative anomalies of Zr and Sr are observed. Some U spikes (Fig. 5b) may be due to surface alterations because U and Th show incoherent behaviors (Fig. 5a), although Alard et al. (1998) suggested that U-Th decoupling in xenoliths from Massif Central is related to fluid processes in the lithospheric mantle. The cpx-poor lherzolite (SJXO-8, Yb_n = 0.7 to 1.5) is characterized by a relatively strong light REE (LREE) enrichment [$(La/Yb)_n \sim 10$] and a flat heavy REE (HREE) pattern. They show pronounced negative Ti, Zr, Hf, Nb and Ta anomalies (Fig. 5b).

For convenience, the whole rock data of harzburgites are presented as two types (Fig. 5c-f) following the classification based on REE composition of cpx separates (see next section). The first type (except for DLW-7) is characterized by a relatively flat pattern with only a slight enrichment of LREE over HREE ($(La/Yb)_n$= 1 to 2.2; Figure 5c). La contents are relatively low (La_n = 0.6 to 1). Positive Ti and Hf, and negative Sr and Nb anomalies characterize the PM-normalized spiderdiagram (Fig. 5d). An exception is found for DLW-7, which shows a relatively higher enrichment of LREE than other samples in this group. Another type shows a relatively high La content (La_n = 1 to 12) and a slightly U-shaped REE pattern [$(Gd/Yb)_n$ = 0.5 to 0.8] (Fig. 5e). Many samples in this second type show negative Nb and sometimes Ta anomalies as well. Negative Sr and positive Ti anomalies are present for DYS-1, DYS-21 and DLW-4, but no such anomalies are observed for DYS-8 which is marked by positive Zr-Hf anomalies (Fig. 5f). DLW-8 has higher REE concentrations than other samples. This sample is characterized by LREE-enrichment and by negative Ti, Zr, Hf, Nb and Ta anomalies.

Table 1. Representative mineral chemistry of peridotite xenoliths from Huinan

SiO_2	TiO_2	Al_2O_3	Cr_2O_3	FeO	MnO	MgO	CaO	Na_2O	K_2O	Total	Sample	Mineral	Cr#	Mg#
Lherzolites														
51.07	0.47	5.55	0.62	3.11	0.05	15.62	22.20	1.16	0.00	99.87	SJXO-1	opx	0.07	0.899
54.70	0.08	3.63	0.21	6.87	0.17	33.59	0.90	0.06	0.01	100.22	SJXO-1	opx	0.04	0.897
0.05	0.11	55.12	9.65	12.37	0.04	22.15	0.01	0.03	0.00	99.51	SJXO-1	sp	0.11	0.761
39.75	0.00	0.60	0.16	9.56	0.09	50.82	0.14	0.04	0.01	101.18	SJXO-2	ol		0.905
50.28	0.64	5.94	0.95	3.16	0.01	17.72	20.43	0.90	0.01	100.05	SJXO-2	cpx	0.10	0.909
53.83	0.09	4.10	0.44	6.12	0.09	34.93	0.89	0.09	0.02	100.59	SJXO-2	opx	0.07	0.910
0.10	0.50	49.89	16.80	11.54	0.24	20.68	0.01	0.00	0.00	99.76	SJXO-2	sp	0.18	0.762
40.70	0.01	0.01	0.00	8.41	0.00	51.75	0.04	0.00	0.00	100.93	SJXO-3	ol		0.916
51.38	0.40	4.13	0.74	2.27	0.00	15.65	22.78	1.02	0.01	98.38	SJXO-3	cpx	0.11	0.925
54.77	0.06	1.59	0.22	5.77	0.12	35.81	0.40	0.00	0.00	98.74	SJXO-3	opx	0.09	0.917
0.04	0.12	47.76	18.97	11.97	0.20	19.97	0.00	0.00	0.01	99.04	SJXO-3	sp	0.21	0.748
39.76	0.03	0.00	0.02	10.38	0.03	50.01	0.00	0.00	0.02	100.25	SJXO-4	ol		0.896
51.22	0.35	5.83	0.66	2.66	0.00	15.07	22.66	1.54	0.01	99.99	SJXO-4	cpx	0.07	0.910
53.94	0.06	3.64	0.34	6.75	0.10	33.98	0.38	0.02	0.00	99.21	SJXO-4	opx	0.06	0.900
0.04	0.04	57.35	10.06	10.68	0.11	20.38	0.02	0.01	0.00	98.70	SJXO-4	sp	0.11	0.773
39.77	0.00	0.00	0.01	11.90	0.26	48.96	0.07	0.00	0.00	100.98	SJXO-6	ol		0.880
50.96	0.14	4.83	0.65	4.28	0.11	17.49	20.17	1.06	0.01	99.72	SJXO-6	cpx	0.08	0.879
53.05	0.21	5.11	0.39	7.02	0.00	32.49	1.09	0.07	0.00	99.42	SJXO-6	opx	0.05	0.892
0.06	0.71	47.57	13.86	16.73	0.08	20.14	0.02	0.00	0.00	99.18	SJXO-6	sp	0.16	0.682
38.87	0.00	0.05	0.02	10.01	0.07	50.88	0.11	0.00	0.00	100.01	SJXO-8	ol		0.901
52.05	0.01	4.44	0.70	3.15	0.02	17.86	20.66	0.86	0.00	99.76	SJXO-8	cpx	0.10	0.910
54.70	0.00	1.75	0.25	5.97	0.07	35.60	0.53	0.00	0.03	98.91	SJXO-8	opx	0.09	0.914
0.05	0.01	49.21	17.83	12.62	0.12	20.75	0.01	0.00	0.00	100.60	SJXO-8	sp	0.20	0.746
39.32	0.01	0.06	0.06	9.98	0.02	50.71	0.09	0.01	0.05	100.29	DLW-9	ol		0.901
50.75	0.42	5.41	0.61	2.80	0.03	15.96	22.03	1.26	0.00	99.27	DLW-9	cpx	0.07	0.910
53.50	0.08	4.81	0.35	6.27	0.10	34.30	0.57	0.04	0.03	100.03	DLW-9	opx	0.05	0.907
0.00	0.08	58.20	10.65	10.91	0.00	21.41	0.00	0.00	0.00	101.25	DLW-9	sp	0.11	0.778
39.76	0.00	0.01	0.03	8.94	0.01	51.22	0.02	0.02	0.00	100.00	DYS-12	ol		0.911
50.43	0.42	5.73	0.50	2.70	0.00	16.36	22.18	1.19	0.00	99.51	DYS-12	cpx	0.05	0.915
53.32	0.10	3.74	0.26	6.26	0.18	34.73	0.52	0.05	0.00	99.14	DYS-12	opx	0.04	0.908
0.03	0.03	57.01	10.69	10.95	0.21	21.79	0.00	0.03	0.01	100.74	DYS-12	sp	0.11	0.780
38.50	0.03	0.00	0.03	10.25	0.02	50.88	0.02	0.00	0.00	99.71	DYS-5	ol		0.898
51.19	0.51	6.20	0.46	2.64	0.05	15.18	22.52	1.72	0.00	100.48	DYS-5	cpx	0.05	0.911
54.76	0.08	3.25	0.20	6.81	0.16	34.09	0.39	0.04	0.00	99.78	DYS-5	opx	0.04	0.899
0.00	0.05	55.92	8.97	12.28	0.12	22.33	0.01	0.00	0.00	99.67	DYS-5	sp	0.10	0.764
39.72	0.00	0.00	0.05	10.75	0.04	49.29	0.08	0.03	0.00	99.97	DYS-9	ol		0.891
51.24	0.47	4.80	0.61	3.26	0.04	16.62	22.18	1.04	0.02	100.28	DYS-9	cpx	0.08	0.901
52.72	0.04	3.35	0.37	7.20	0.13	34.95	0.78	0.09	0.00	99.64	DYS-9	opx	0.07	0.896
0.03	0.18	47.95	18.50	14.14	0.33	18.50	0.03	0.07	0.02	99.74	DYS-9	sp	0.21	0.700
Harzburgites														
40.00	0.00	0.05	0.03	9.33	0.14	50.39	0.13	0.00	0.00	100.07	DLW-3	ol		0.906
51.11	0.19	5.76	1.27	3.69	0.08	17.67	19.14	0.95	0.00	99.86	DLW-3	cpx	0.13	0.895
54.66	0.05	1.97	0.37	6.35	0.07	34.27	0.92	0.05	0.00	98.69	DLW-3	opx	0.11	0.906
0.09	0.14	39.43	26.45	14.02	0.23	19.27	0.00	0.00	0.00	99.63	DLW-3	sp	0.31	0.710
38.94	0.00	0.07	0.01	9.57	0.04	51.69	0.01	0.00	0.01	100.33	DLW-4	ol		0.906
51.14	0.38	4.10	0.67	2.55	0.09	16.72	22.39	0.95	0.00	98.99	DLW-4	cpx	0.10	0.921
54.64	0.13	1.44	0.28	5.72	0.16	34.80	0.50	0.07	0.01	97.75	DLW-4	opx	0.12	0.916
0.04	0.37	41.68	25.83	12.05	0.23	20.32	0.00	0.00	0.00	100.52	DLW-4	sp	0.29	0.750
39.27	0.00	0.04	0.00	8.78	0.19	52.46	0.08	0.02	0.00	100.84	DLW-5	ol		0.914
49.91	0.49	7.23	0.99	2.30	0.12	16.01	20.82	1.08	0.15	99.08	DLW-5	cpx	0.08	0.925
54.70	0.13	1.99	0.39	5.76	0.07	35.51	0.51	0.12	0.04	99.21	DLW-5	opx	0.12	0.917
0.02	0.31	37.68	29.38	12.29	0.22	20.12	0.00	0.00	0.00	100.02	DLW-5	sp	0.34	0.745
39.57	0.01	0.02	0.09	8.68	0.00	50.80	0.04	0.00	0.00	99.20	DLW-6	ol		0.913
52.38	0.40	1.50	0.59	2.61	0.00	18.10	23.82	0.59	0.00	99.99	DLW-6	cpx	0.21	0.925
55.73	0.08	1.04	0.32	5.87	0.12	35.51	0.45	0.02	0.01	99.14	DLW-6	opx	0.17	0.915
0.00	0.44	32.50	33.46	15.43	0.28	17.27	0.00	0.00	0.00	99.39	DLW-6	sp	0.41	0.666
40.45	0.04	0.00	0.08	9.03	0.17	50.65	0.05	0.00	0.00	100.47	DLW-7	ol		0.909
51.09	0.24	4.38	0.89	2.22	0.00	16.51	22.87	0.98	0.01	99.19	DLW-7	cpx	0.12	0.930
55.40	0.06	1.67	0.30	5.87	0.06	35.18	0.41	0.04	0.00	99.00	DLW-7	opx	0.11	0.914
0.00	0.13	46.05	22.89	12.11	0.19	20.32	0.00	0.00	0.00	101.69	DLW-7	sp	0.25	0.749
39.44	0.02	0.00	0.04	9.17	0.00	51.66	0.07	0.00	0.00	100.40	DLW-8	ol		0.909
51.64	0.14	3.75	1.35	2.76	0.06	16.40	20.85	1.62	0.02	98.59	DLW-8	cpx	0.19	0.914
54.48	0.06	1.98	0.48	5.28	0.07	35.13	0.82	0.12	0.00	98.42	DLW-8	opx	0.14	0.922
0.00	0.14	29.17	39.38	15.30	0.35	16.07	0.00	0.01	0.00	100.41	DLW-8	sp	0.48	0.652
39.94	0.00	0.01	0.15	9.12	0.07	50.05	0.03	0.00	0.01	99.37	DYS-1	ol		0.907
51.28	0.51	4.58	1.19	2.61	0.02	16.36	21.28	1.16	0.00	98.99	DYS-1	cpx	0.15	0.918

(continued)

Table 1. (Continued)

SiO_2	TiO_2	Al_2O_3	Cr_2O_3	FeO	MnO	MgO	CaO	Na_2O	K_2O	Total	Sample	Mineral	Cr#	Mg#
54.67	0.11	1.63	0.46	5.73	0.00	35.84	0.60	0.07	0.00	99.11	DYS-1	opx	0.16	0.918
0.04	0.28	35.14	31.47	13.95	0.24	18.12	0.02	0.05	0.00	99.31	DYS-1	sp	0.38	0.698
39.68	0.01	0.02	0.05	8.83	0.12	50.82	0.10	0.01	0.02	99.65	DYS-2	ol		0.911
51.63	0.31	4.59	1.38	2.47	0.08	16.04	21.05	1.56	0.01	99.12	DYS-2	opx	0.17	0.920
55.14	0.12	1.70	0.49	5.47	0.10	35.53	0.91	0.17	0.02	99.65	DYS-2	opx	0.16	0.920
0.04	0.54	36.51	29.65	14.05	0.31	19.19	0.00	0.00	0.00	100.28	DYS-2	sp	0.35	0.709
40.28	0.00	0.00	0.00	8.50	0.00	51.25	0.09	0.00	0.00	100.12	DYS-3	ol		0.915
50.98	0.34	3.67	1.14	2.44	0.00	17.54	22.07	1.04	0.00	99.21	DYS-3	cpx	0.17	0.928
55.22	0.16	1.51	0.41	5.36	0.12	35.51	0.65	0.04	0.03	99.00	DYS-3	opx	0.15	0.922
0.02	0.44	33.49	33.48	13.78	0.09	18.41	0.01	0.00	0.00	99.73	DYS-3	sp	0.40	0.704
38.69	0.00	0.01	0.04	9.11	0.08	50.87	0.05	0.01	0.00	98.87	DYS-4	ol		0.909
51.41	0.30	5.27	0.74	2.90	0.08	15.75	21.89	1.20	0.01	99.54	DYS-4	cpx	0.09	0.906
54.16	0.03	3.30	0.30	5.98	0.00	33.16	0.69	0.10	0.02	97.72	DYS-4	opx	0.06	0.908
0.06	0.23	49.55	20.77	12.34	0.24	17.94	0.00	0.02	0.00	101.14	DYS-4	sp	0.22	0.722
40.76	0.03	0.00	0.03	9.17	0.19	50.42	0.04	0.02	0.00	100.65	DYS-6	ol	1.00	0.907
50.58	0.18	3.76	1.42	2.34	0.08	15.83	21.66	1.29	0.02	97.14	DYS-6	cpx	0.20	0.924
0.07	0.24	32.89	37.51	13.15	0.28	17.09	0.00	0.00	0.00	101.22	DYS-6	sp	0.43	0.698
39.36	0.02	0.02	0.00	8.55	0.02	51.88	0.08	0.00	0.02	99.96	DYS-7	ol		0.915
51.45	0.49	4.94	1.42	2.63	0.07	17.63	20.12	1.43	0.00	100.18	DYS-7	cpx	0.16	0.923
54.96	0.15	2.63	0.32	5.35	0.00	35.07	0.60	0.07	0.00	99.15	DYS-7	opx	0.08	0.921
0.07	0.65	34.18	32.19	13.68	0.24	19.01	0.00	0.00	0.00	100.03	DYS-7	sp	0.39	0.712
40.30	0.02	0.06	0.01	9.09	0.06	49.65	0.10	0.04	0.00	99.33	DYS-8	ol		0.907
52.45	0.17	4.08	1.10	2.78	0.12	17.58	20.09	1.35	0.00	99.72	DYS-8	cpx	0.15	0.918
56.26	0.08	1.35	0.48	5.58	0.00	34.92	0.79	0.08	0.01	99.54	DYS-8	opx	0.19	0.918
0.06	0.29	33.65	36.22	13.56	0.25	17.45	0.00	0.00	0.00	101.48	DYS-8	sp	0.42	0.696
39.97	0.00	0.03	0.02	8.63	0.00	52.11	0.07	0.00	0.03	100.86	DYS-21	ol		0.915
51.76	0.27	5.07	1.40	2.98	0.07	17.08	20.75	1.24	0.02	100.64	DYS-21	cpx	0.16	0.911
54.37	0.11	1.93	0.53	5.57	0.07	35.47	1.02	0.13	0.01	99.20	DYS-21	opx	0.16	0.919
0.04	0.30	34.84	33.04	12.95	0.39	18.63	0.00	0.00	0.00	100.18	DYS-21	sp	0.39	0.719

4.3. Trace Elements in Clinopyroxene Separates

Clinopyroxene separates from lherzolites generally display chondrite-normalized REE patterns that mimic those of the bulk rocks (Table 3, Fig. 6a). All the lherzolite cpx, except two, are depleted in the LREE [i.e., $(La/Yb)_n = 0.1$ to 0.6]. Depletion is also noted for Nb and Ta. These cpx possess negative Ti, and to a lesser degree, negative Zr anomalies relative to the neighbouring REEs (Fig. 6). U and Th concentrations are elevated (except for SJXO-4) possibly due to enrichment processes. Cpx in cpx-poor lherzolite SJXO-8 shows considerably lower HREE contents compared to the majority of lherzolite cpx. It is characterized by a strong enrichment in LREE, a flat HREE pattern and negative anomalies of Nb, Ta, Hf and Ti.

Cpx in harzburgites show REE patterns that are distinct from those of their respective whole rocks. Two types of REE patterns in cpx can be distinguished (Fig. 6c, e). The first is a convex-upward pattern with a maximum at Sm or Eu. Cpx with this REE pattern has a LREE content similar to those of LREE-depleted cpx from lherzolites, but their HREE contents are lower than those for lherzolite cpx (Fig. 6c). Cpx from DYS-2, DYS-3 and DYS-7 show even higher MREE contents than cpx in lherzolites (Fig. 6c). In PM-normalized diagrams, these cpx are similar to lherzolite cpx except that they have less obvious Zr-Hf anomalies and more ubiquitous U-Th enrichments (Fig. 6d). The second type differs from the first type in showing LREE enrichment of varying degrees (Fig. 6e). While DYS-8 shows a steadily enriched pattern, others show spoon-shaped LREE patterns. The enriched REE pattern of DYS-8 differs from those of LREE-enriched cpx from lherzolites in the absence of Hf anomalies, a less pronounced negative Ti anomaly and a higher LREE concentration.

Yb contents in cpx from the Huinan harzburgites (1 to 2 ppm) are significantly higher than those in cpx of the harzburgites which have been interpreted as residues of partial melting ("residual harzburgites," 0.2 to 0.4 ppm; Shi et al., 1998; Norman, 1998; Xu et al., 1998b). They are even higher than in cpx from the cpx-poor lherzolite (SJXO-8). The difference between the Huinan harzburgites and "residual harzburgites" is more important for the MREE. These are inconsistent with the modal composition of the harzburgites, if the harzburgites are residues of high degrees of partial melting. Ti contents in cpx of as much as 5000 ppm are also striking, because cpx from "residual" harzburgites generally have Ti contents <1000 ppm (Johnson et al., 1990; Shi et al., 1998).

4.4. Sr-Nd Isotopes in Clinopyroxene Separates

The lherzolite cpx have a wide range in isotopes ($\varepsilon_{Nd} = +18.5$ to -0.2 and $^{87}Sr/^{86}Sr = 0.7022$ to 0.7047; Table 4) ranging from ratios similar to those of depleted mantle (Zindler and Hart, 1986) to values slightly more enriched than the Bulk Earth (Fig. 7a). This is typical of suites of spinel peridotite xenoliths from single localities (e.g., Menzies et al., 1985; Stosch and Lugmair, 1986; Stosch et al., 1986; McDonough and McCulloch, 1987; Roden et al., 1988; Ionov et al., 1992; Xu et al., 1998b), indicating large isotopic heterogeneity in the continental lithospheric mantle. All the lherzolite cpx (except

Table 2. Representative major and trace element composition of whole rock peridotites from Huinan

	Lherzolites								
	SJXO-1	SJXO-4	SJXO-6	SJXO-7	SJXO-8	DYS-5	DYS-12	DLW-9	HN-07
SiO_2	43.57	42.97	42.88	41.86	44.37	41.63	42.69	43.47	43.15
TiO_2	0.11	0.08	0.11	0.10	0.02	0.13	0.11	0.08	0.10
Al_2O_3	3.29	2.91	3.06	3.70	2.05	3.64	3.72	2.81	4.02
Fe_2O_3	1.55	1.64	1.40	2.72	1.52	1.78	1.38	2.49	1.84
FeO	9.26	8.84	9.40	9.56	7.98	7.46	9.23	6.79	8.61
MnO	0.16	0.15	0.16	0.15	0.15	0.17	0.16	0.15	0.15
MgO	37.45	38.87	38.65	37.43	40.90	40.88	37.46	40.52	37.34
CaO	3.49	3.51	3.04	2.93	1.99	3.23	3.85	2.45	3.16
Na_2O	0.20	0.21	0.20	0.21	0.13	0.18	0.21	0.19	0.23
K_2O	0.01	0.01	0.01	0.01	0.01	0.02	0.01	0.01	0.01
P_2O_3	0.04	0.03	0.04	0.05	0.05	0.08	0.02	0.07	0.07
H_2O^+	0.57	0.72	0.79	1.21	0.58	0.62	0.88	0.54	0.77
Total	99.70	99.94	99.74	99.97	99.63	99.82	99.72	99.57	99.45
Modal compositions									
Ol	56.2	57.6	57.3	59.0	51.5	61.8	48.6	56.4	
Cpx	13.3	15.4	13.7	15.5	8.4	14.0	17.3	10.2	
Opx	27.5	25.0	25.6	21.0	38.1	20.5	31.1	32.2	
SP	3.0	2.0	2.3	4.4	2.0	3.8	3.0	1.2	
ICP-MS analyses									
Ti	614	463	595	585	130	662	458	459	602
Cr	3291	3306	3479	3210	3861	3339	2550	2909	4291
Ni	1684	1707	1626	1632	1977	1689	1335	1896	1876
Rb	0.19	0.16	0.22	0.22	0.21	0.16	0.18	0.19	0.19
Sr	5.99	3.33	14.03	5.39	6.01	7.66	3.64	5.55	3.81
Y	3.04	2.68	2.70	2.91	0.61	3.05	2.35	2.14	3.36
Zr	3.37	2.37	6.28	3.25	3.56	5.39	2.37	3.81	2.59
Nb	0.20	0.15	0.36	0.15	0.66	0.15	0.11	0.13	0.14
Ba	3.90	2.91	4.03	3.93	3.85	3.20	3.21	3.07	4.85
Hf	0.12	0.10	0.17	0.14	0.07	0.18	0.12	0.13	0.14
Ta	0.03	0.02	0.04	0.02	0.05	0.01	0.01	0.01	0.01
Th	0.03	0.02	0.13	0.11	0.13	0.02	0.02	0.03	0.02
U	0.02	0.01	0.03	0.04	0.03	0.01	0.01	0.02	0.02
La	0.35	0.20	1.47	0.32	0.80	0.21	0.13	0.18	0.20
Ce	0.83	0.41	3.61	0.57	1.52	0.61	0.37	0.51	0.39
Pr	0.15	0.08	0.47	0.12	0.17	0.12	0.08	0.09	0.09
Nd	0.75	0.42	1.91	0.62	0.59	0.68	0.42	0.50	0.48
Sm	0.23	0.17	0.39	0.22	0.09	0.24	0.16	0.16	0.21
Eu	0.08	0.06	0.12	0.08	0.03	0.09	0.06	0.06	0.08
Gd	0.29	0.24	0.37	0.28	0.08	0.31	0.22	0.20	0.29
Tb	0.06	0.05	0.07	0.06	0.01	0.06	0.05	0.04	0.07
Dy	0.43	0.38	0.40	0.41	0.09	0.46	0.35	0.30	0.51
Ho	0.11	0.09	0.09	0.10	0.02	0.11	0.09	0.08	0.13
Er	0.32	0.28	0.28	0.30	0.07	0.32	0.26	0.22	0.39
Tm	0.05	0.04	0.04	0.05	0.01	0.05	0.04	0.04	0.06
Yb	0.34	0.28	0.29	0.31	0.09	0.34	0.27	0.25	0.41
Lu	0.05	0.05	0.05	0.05	0.02	0.06	0.04	0.04	0.07

Note: the modal proportions of minerals were calculated using a least squares method combining the bulk rock compositions and electron microprobe analyses of the minerals.

SJXO-4) define a good negative correlation in Sr-Nd isotopic space (Fig. 7a). The LREE-enriched lherzolite cpx appear to be more isotopically enriched than the LREE-depleted samples and are isotopically similar to the host basalts. SJXO-4 plots well off the mantle array, displaying a higher ε_{Nd} for its Sr isotopic ratio. Similar isotopic decoupling has been widely reported in worldwide occurrences (e.g., Stosch and Lugmair, 1986; Galer and O'Nions, 1989; Ionov et al., 1992; Xu et al., 1998b). In the Sm-Nd isochron diagram (Fig. 7b), three LREE-depleted samples (DYS-5, DLW-9 and SJXO-1) define a line passing through the Bulk Earth point. Linear regression of the data yields an age of 1.6 Ga. SJXO-4 and DYS-12 define a line passing through the Bulk-Earth corresponding to an age of 1.0 Ga. If these ages are geologically meaningful, they could reflect multiple melting events. The positive correlation defined by all cpxs from lherzolites (both LREE-depleted and -enriched) does not intersect the Bulk Earth point nor the present-day oceanic depleted mantle (shaded field, Fig. 7b). This trend is believed to have no chronological significance because of the trace element evidence for introduction of LREE-rich component in some samples (e.g., SJXO-6 and SJXO-8). This correlation probably reflects mixing between a depleted mantle source with high ε_{Nd} and high Sm/Nd ratio and an enriched end-member with lower ε_{Nd} and low Sm/Nd.

With the exception of DLW-4, the harzburgite cpx shows a

Harzburgites												
DYS-1	DYS-2	DYS-3	DYS-6	DYS-7	DYS-8	DYS-21	DLW-3	DLW-4	DLW-5	DLW-6	DLW-7	DLW-8
43.72	42.89	42.25	41.46	41.73	41.73	42.84	42.77	42.39	41.51	42.13	42.94	42.07
0.09	0.07	0.09	0.02	0.05	0.03	0.06	0.05	0.08	0.06	0.06	0.05	0.05
1.80	1.52	1.37	1.30	0.57	1.11	1.56	1.65	1.55	1.44	1.19	1.74	1.20
1.06	1.05	1.87	1.88	1.88	0.98	1.57	1.84	1.52	1.24	1.30	1.74	2.23
7.61	7.25	7.85	9.16	8.21	8.71	7.56	9.49	8.68	8.29	8.39	9.15	9.50
0.14	0.14	0.15	0.15	0.15	0.15	0.14	0.16	0.14	0.15	0.14	0.15	0.15
43.41	44.84	44.36	44.12	44.72	45.30	43.28	41.49	43.31	44.78	45.01	41.72	42.22
1.17	1.05	0.94	1.17	1.05	0.94	1.17	1.40	1.05	1.17	0.82	1.28	1.17
0.14	0.11	0.09	0.10	0.08	0.09	0.14	0.10	0.18	0.09	0.07	0.10	0.15
0.02	0.03	0.03	0.04	0.01	0.01	0.01	0.01	0.01	0.01	0.01	0.02	0.04
0.08	0.12	0.12	0.08	0.07	0.06	0.14	0.04	0.07	0.03	0.06	0.06	0.08
0.29	0.63	0.37	0.69	1.70	0.40	1.42	0.74	0.53	0.77	0.48	0.57	0.71
99.53	99.51	99.49	100.17	100.22	99.51	99.89	99.74	99.51	99.54	99.66	99.52	99.57
63.8	69.6	70.2	77.8	75.3	81.2	62.6	62.2	63.3	69.9	71.6	61.7	62.5
4.6	3.7	3.2	4.0	2.7	3.8	4.0	5.7	4.0	5.0	2.7	5.1	4.2
29.6	24.8	24.6	13.8	21.1	13.6	31.9	30.4	30.8	23.5	23.0	30.9	32.1
2.1	2.0	2.0	4.4	1.0	1.4	1.5	1.6	1.9	1.7	2.7	2.2	1.2
520	398	410	216	277	205	261	221	401	320		299	309
3977	3516	4332	3531	1796	2977	3444	3124	2655	4083		4137	4734
1906	1870	1919	2100	1855	2041	1690	1955	1783	2136		1978	2090
0.19	0.34	0.16	0.19	0.16	0.21	0.23	0.30	0.23	0.19		0.60	0.62
4.56	3.45	2.34	12.75	2.26	8.23	4.54	4.95	2.22	2.80		6.47	33.07
0.98	1.07	0.73	0.94	0.54	0.51	0.73	0.75	0.54	0.61		0.79	1.33
3.57	2.59	2.80	3.67	2.22	5.39	2.26	2.88	1.96	1.75		2.43	5.07
0.12	0.11	0.12	0.33	0.15	0.22	0.13	0.42	0.18	0.14		0.25	1.09
4.20	4.50	3.06	5.23	4.01	4.70	4.04	5.26	3.16	3.60		5.97	11.14
0.11	0.09	0.09	0.09	0.07	0.11	0.10	0.07	0.06	0.05		0.08	0.12
0.01	0.01	0.01	0.01	0.01	0.02	0.01	0.03	0.01	0.01		0.02	0.05
0.03	0.06	0.02	0.05	0.02	0.05	0.04	0.10	0.11	0.07		0.09	0.14
0.01	0.02	0.01	0.02	0.01	0.02	0.01	0.02	0.03	0.03		0.04	0.04
0.24	0.16	0.14	0.73	0.18	0.39	0.29	0.44	0.30	0.18		0.33	3.05
0.53	0.31	0.32	1.78	0.39	0.95	0.61	0.89	0.54	0.37		0.68	6.22
0.08	0.06	0.06	0.23	0.06	0.12	0.08	0.12	0.07	0.06		0.10	0.63
0.35	0.27	0.28	1.00	0.27	0.49	0.27	0.46	0.28	0.27		0.44	2.09
0.10	0.10	0.08	0.20	0.07	0.09	0.07	0.09	0.06	0.07		0.10	0.28
0.03	0.04	0.03	0.06	0.02	0.03	0.03	0.03	0.02	0.03		0.03	0.09
0.11	0.12	0.09	0.17	0.08	0.08	0.09	0.10	0.07	0.08		0.10	0.25
0.02	0.02	0.02	0.03	0.01	0.01	0.02	0.02	0.01	0.01		0.02	0.04
0.14	0.16	0.11	0.18	0.09	0.09	0.11	0.11	0.08	0.10		0.12	0.23
0.03	0.04	0.03	0.03	0.02	0.02	0.03	0.03	0.02	0.02		0.03	0.05
0.10	0.11	0.08	0.09	0.06	0.06	0.08	0.09	0.06	0.07		0.09	0.14
0.01	0.02	0.01	0.01	0.01	0.01	0.01	0.01	0.01	0.01		0.01	0.02
0.09	0.11	0.08	0.09	0.06	0.07	0.10	0.11	0.07	0.08		0.10	0.14
0.02	0.02	0.01	0.02	0.01	0.01	0.02	0.02	0.01	0.01		0.02	0.02

relatively restricted range in isotopes (ε_{Nd} = +6.4 to +0.6 and $^{87}Sr/^{86}Sr$ = 0.7032 to 0.7043). It is noted that cpx, with convex-upward REE patterns [$(La/Nd)_n<1$], lie near the negative correlation defined by the lherzolites. Specifically, the isotopic composition of some cpx overlaps with that of the host basalts (Fig. 7a). In contrast, LREE-enriched cpx [$(La/Nd)_n>1$] tend to plot below the mixing line (Fig. 7a). The harzburgites do not define any clear correlation between Sm/Nd and ε_{Nd} because of the small variation of ε_{Nd} over a wide range of Sm/Nd (Fig. 7b). It is possible that the LREE-enrichment occurred very recently such that insufficient time has elapsed for the elemental ratios to register in the Sr and Nd isotope ratios.

DLW-4 is distinct from the other harzburgites in having an extremely high $^{87}Sr/^{86}Sr$ (0.711318) and a moderately low ε_{Nd} (+2.4). Such an isotopic composition is enigmatic because DLW-4 is petrographically similar to other samples. This cannot be related to a contamination problem because duplicate analyses yield virtually identical results (Table 4). Similarly extreme Sr-Nd isotopic compositions have been reported for mantle xenoliths from South Africa, East Africa and Scotland (e.g., Menzies and Murthy, 1980, Cohen et al., 1984; Menzies and Halliday, 1988; Hawkesworth et al., 1990). It is noted that the high $^{87}Sr/^{86}Sr$ in DLW-4 is "unsupported" by its Rb/Sr ratio, which is low and is indistinguishable from those of other samples (Table 3).

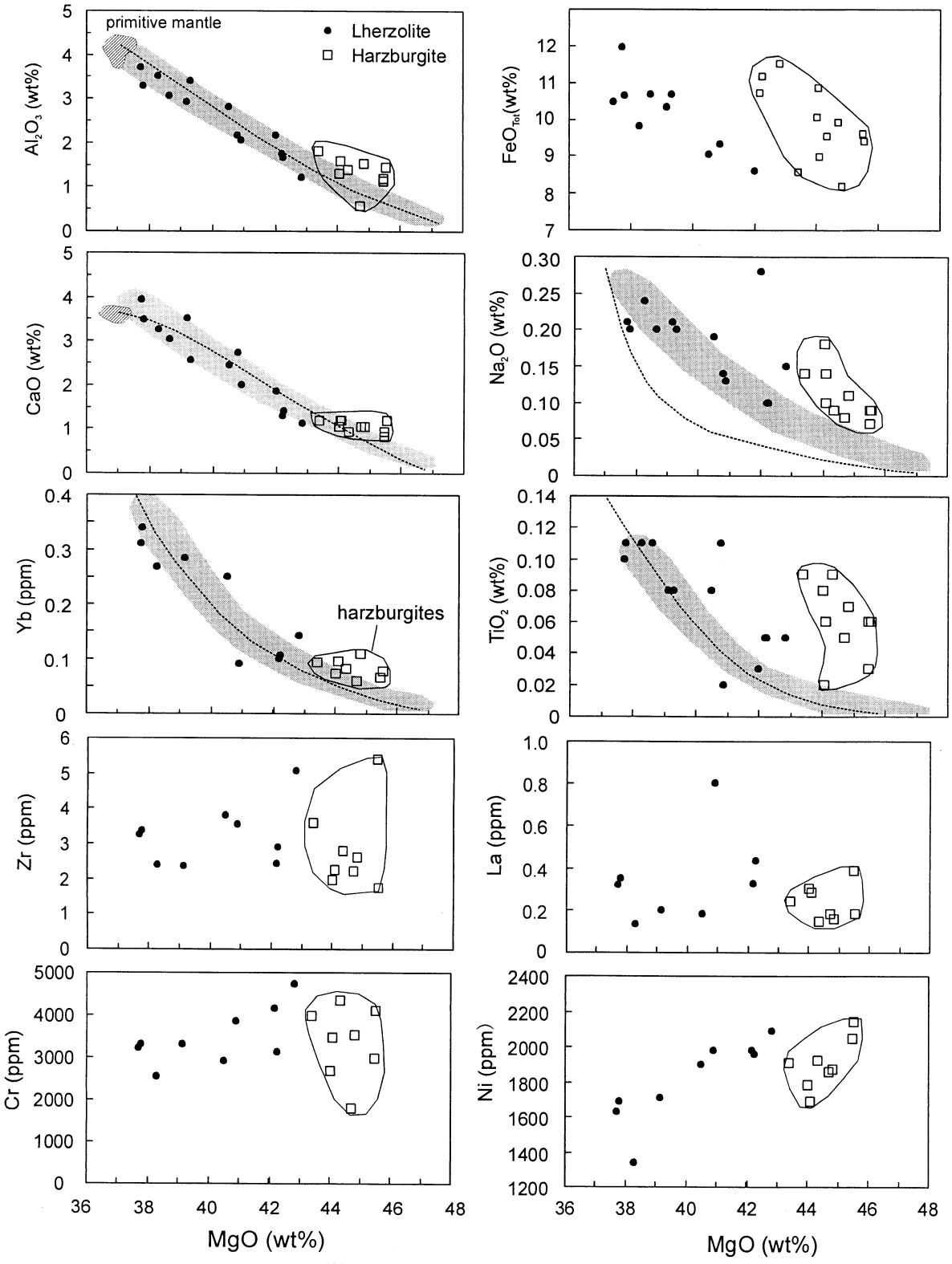

Fig. 4. Plots of CaO, Al_2O_3, FeO, Na_2O, selected incompatible elements (TiO_2, Yb, La, Yb, Zr) and compatible elements (Cr and Ni) against MgO for peridotite xenoliths from Huinan. The shaded fields represent the compositional range for worldwide peridotites (Takazawa et al., 2000). Dashed line is near-fractional melting model trend of a starting source of primitive spinel peridotites using the model of Niu (1997)(after Takazawa et al., 2000). Diagonally hatched areas are primitive mantle compositions (Jagoutz et al., 1979; Hart and Zindler, 1986).

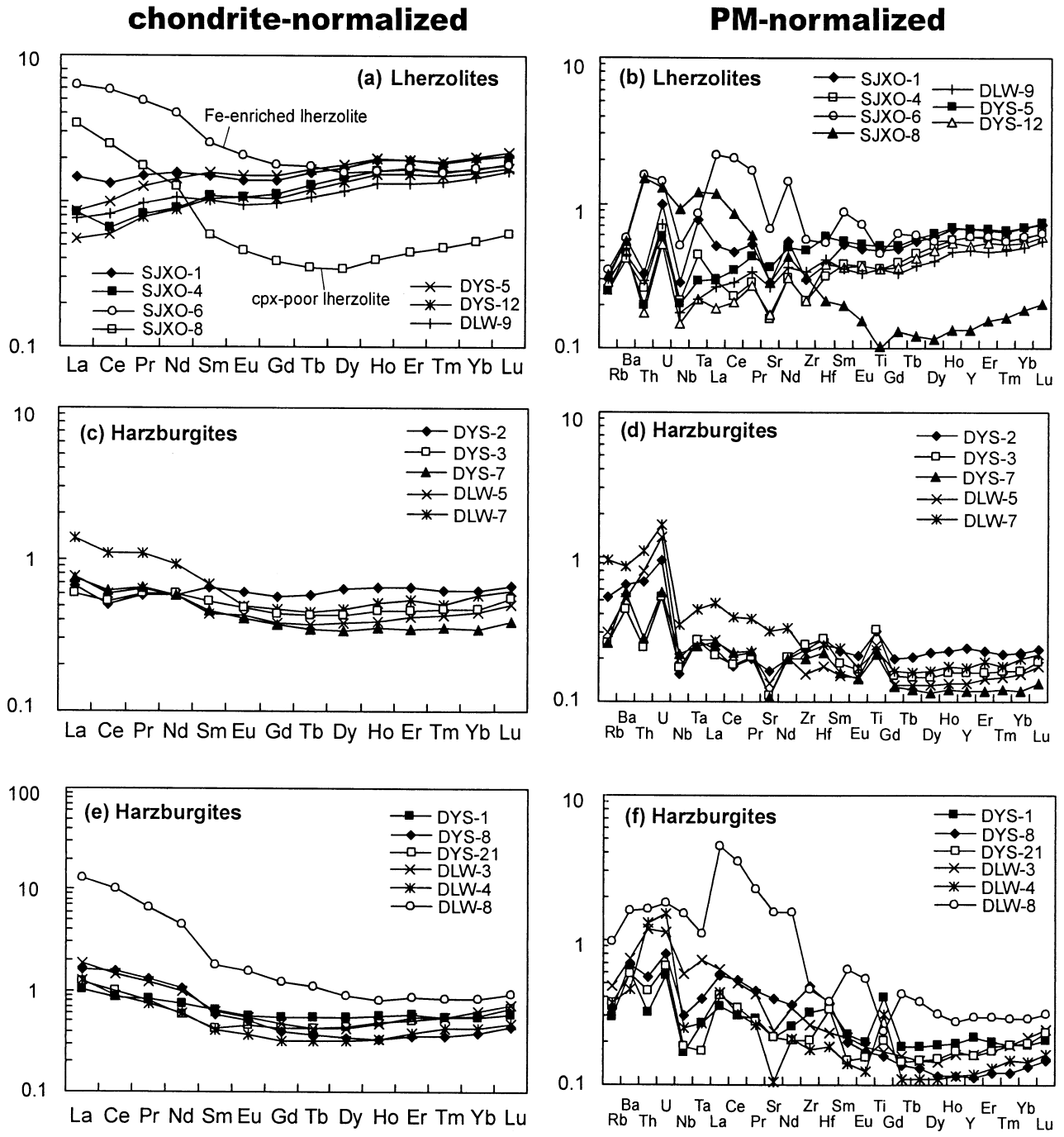

Fig. 5. REE and trace element abundances in whole rocks of Huinan peridotites. On the left, the REE patterns normalized by chondrite values (Sun and McDonough, 1989). On the right hand are spiderdiagrams with trace elements normalized to primitive mantle values (Sun and McDonough, 1989).

5. DISCUSSION

5.1. Lherzolites—Samples of the Lithospheric Mantle

The inverse correlations between CaO, Al_2O_3, Yb and MgO in the lherzolites from Huinan are qualitatively consistent with variable extraction of basaltic melts (Frey et al., 1985; McDonough and Frey, 1989; Takazawa et al., 2000). Figure 4 compares the major element compositions of the samples with polybaric fractional model trends of primitive mantle (Niu, 1997). The Al_2O_3-MgO and CaO-MgO trends are close to the calculated ones based on experimental results. These lherzolites can thus be interpreted as refractory residues left after the extraction of basalts. Comparison of Y and Ti contents in lherzolite cpx and the modeled melting trend (Fig. 8a) further

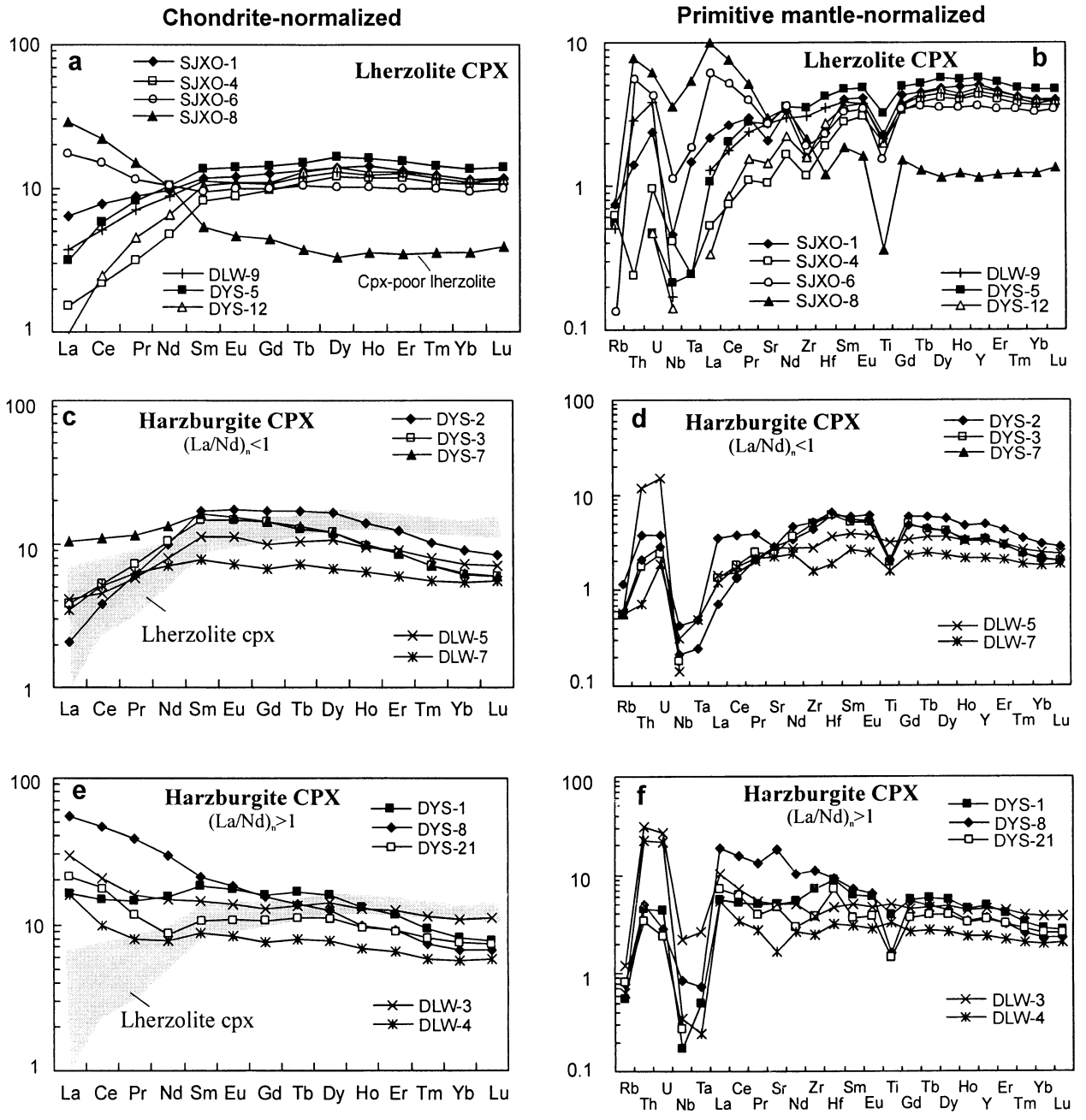

Fig. 6. REE and trace element abundances in clinopyroxenes from Huinan peridotites.

indicates that the degree of melting for the Huinan lherzolites varies between 0 and 15%. The most depleted isotopic composition (ε_{Nd} = +18, SJXO-4) of the Huinan lherzolites is beyond that of MORB (Zindler and Hart, 1986). In this sense, the Huinan lherzolites are not equivalent to the suboceanic mantle beneath spreading ridges. High ε_{Nd} has frequently been reported for xenoliths from continental settings (Stosch and Lugmair, 1986; Stosch et al., 1986; McDonough and McCulloch, 1987; Xu et al., 1998b; Fan et al., 2000b). The Nd isotopic composition might reflect time-integrated isotopic evolution of residual peridotites in non-convective reservoirs like the lithosphere. Since the LREE-depleted lherzolites (i.e., SJXO-4 and DYS-5) represent the mantle fragments that were not affected by any significant metasomatic alteration, they may retain important information about the mantle protolith and age of depletion. The calculated Nd model age for these samples using a single stage model from a primitive mantle is between 1.0 to 1.6 Ga, indicating a Proterozoic age of partial melting (Fig. 7b). This depletion event can be envisaged as the initial stabilization of the lithospheric mantle in conjunction with crust formation (Stosch et al., 1986; McDonough and McCulloch, 1987; Xu et al., 1998b). Because no signs of metasomatism are observed for

Table 3. Trace element concentration in clinopyroxenes from Huinan peridotites (ppm)

	Lherzolites							Harzburgites									
	SJXO-1	SJXO-4	SJXO-6	SJXO-8	DYS-5	DYS-12	DLW-9	DYS-1	DYS-2	DYS-3	DYS-7	DYS-8	DYS-21	DLW-3	DLW-4	DLW-5	DLW-7
Sc	76	77	69	65	82	80	79	103	94	92	90	109	95	152	85	108	82
Ti	2953	2567	1966	470	4205	2584	2742	5091	2698	2536	2637	2077	1851	6619	4295	4057	2088
V	302	291	225	180	321	305	304	295	297	185	183	301	173	662	296	318	204
Cr	6577	6541	4547	8263	6655	6115	7536	13050	15223	10766	10784	14486	13915	19411	10348	12150	9523
Mn	568	495	613	513	529	557	578	532	536	508	492	607	562	532	461	488	484
Co	25	21	25	26	20	23	25	24	26	26	25	28	26	51	22	24	23
Ni	359	312	453	410	283	338	382	366	406	406	378	414	407	678	331	368	360
Ga	3.87	3.47	2.99	2.6	4.08	3.49	3.67	3.78	3.89	3.09	3.18	4.61	3.83	6.33	3.52	3.23	2.61
Rb	0.47	0.39	0.09	0.48	0.35	0.34	0.32	0.35	0.74	0.35	0.37	0.50	0.51	0.76	0.40	0.37	0.36
Sr	44.10	22.17	56.79	63.05	56.90	30.46	58.01	104.99	59.77	49.88	59.68	387.85	100.4	105.26	35.17	58.26	46.84
Y	22.95	19.64	16.19	5.20	25.69	21.82	20.27	22.18	22.47	15.27	15.8	16.45	15.73	20.49	10.89	14.9	9.91
Zr	17.73	13.08	20.98	23.53	39.55	17.82	34.05	80.05	48.95	56.11	57.06	125.05	41.74	42.7	27.35	30.39	18.06
Nb	0.33	0.29	0.80	2.57	0.15	0.10	0.12	0.12	0.15	0.13	0.30	0.61	0.19	1.56	0.25	0.10	0.22
Hf	0.72	0.59	0.70	0.37	1.29	0.84	1.09	2.70	1.89	1.89	2.00	2.89	2.22	1.44	0.99	1.14	0.58
Ta	0.06	0.01	0.08	0.22	0.01			0.02	0.01		0.02	0.03		0.11	0.01		0.02
Th	0.12	0.02	0.46	0.66			0.24	0.39	0.32	0.15	0.18	0.43	0.29	2.61	1.92	1.01	0.06
U	0.05	0.02	0.09	0.13	0.01	0.01	0.08	0.09	0.08	0.05	0.06	0.06	0.05	0.57	0.46	0.31	0.04
La	1.50	0.36	4.13	6.86	0.74	0.23	0.89	3.83	0.49	0.91	2.45	12.90	5.01	7.07	3.77	0.98	0.82
Ce	4.72	1.32	9.13	13.60	3.56	1.50	3.13	9.08	2.35	3.21	6.62	28.22	10.89	12.76	6.09	2.74	3.10
Pr	0.83	0.30	1.10	1.43	0.77	0.43	0.66	1.39	0.57	0.69	1.09	3.62	1.10	1.51	0.75	0.55	0.59
Nd	4.49	2.22	4.80	4.76	4.84	3.04	4.06	7.24	4.59	4.86	6.19	13.93	3.96	6.85	3.63	3.68	3.28
Sm	1.79	1.25	1.44	0.82	2.10	1.58	1.70	2.79	2.58	2.25	2.46	3.24	1.61	2.21	1.35	1.70	1.18
Eu	0.69	0.51	0.57	0.27	0.81	0.63	0.63	1.01	1.01	0.85	0.89	1.07	0.63	0.80	0.48	0.64	0.42
Gd	2.58	1.99	2.04	0.90	2.95	2.23	2.17	3.28	3.48	2.91	2.90	3.23	2.17	2.65	1.58	2.05	1.37
Tb	0.49	0.41	0.39	0.14	0.56	0.48	0.45	0.62	0.63	0.47	0.49	0.52	0.42	0.51	0.30	0.39	0.27
Dy	3.56	3.06	2.58	0.84	4.17	3.50	3.27	4.09	4.23	3.02	3.05	3.17	2.85	3.57	1.96	2.67	1.71
Ho	0.80	0.66	0.57	0.20	0.90	0.73	0.69	0.75	0.78	0.54	0.56	0.56	0.54	0.72	0.39	0.53	0.36
Er	2.21	1.94	1.63	0.57	2.56	2.14	2.08	1.94	2.04	1.41	1.42	1.52	1.52	2.07	1.08	1.47	0.99
Tm	0.31	0.28	0.25	0.09	0.36	0.31	0.30	0.24	0.26	0.18	0.18	0.19	0.21	0.29	0.15	0.20	0.14
Yb	1.96	1.82	1.62	0.61	2.30	1.93	1.87	1.40	1.51	1.04	1.06	1.15	1.28	1.85	0.98	1.23	0.91
Lu	0.30	0.27	0.25	0.10	0.35	0.29	0.29	0.20	0.21	0.15	0.15	0.17	0.19	0.28	0.15	0.18	0.14

Table 4. Sr-Nd isotopic ratios of clinopyroxenes from Huinan peridotites

	$^{87}Sr/^{86}Sr$	$^{147}Sm/^{144}Nd$	$^{143}Nd/^{144}Nd$	ε_{Nd}
Lherzolites				
SJXO-1	0.703311 ± 12	0.241	0.513016 ± 4	7.4
SJXO-4	0.702731 ± 11	0.340	0.513586 ± 4	18.5
SJXO-6	0.703976 ± 10	0.181	0.512888 ± 4	4.9
SJXO-8	0.704770 ± 10	0.104	0.512627 ± 4	−0.2
DYS-5	0.702243 ± 10	0.262	0.513302 ± 4	13.0
DYS-12	0.702217 ± 10	0.314	0.513347 ± 4	13.8
DLW-9	0.702585 ± 10	0.253	0.513213 ± 4	11.2
HN-7	0.703083 ± 14		0.512714 ± 4	1.5
Harzburgites [$(La/Nd)_n<1$]				
DLW-5	0.704075 ± 12	0.217	0.512794 ± 4	3.0
DLW-7	0.704149 ± 9	0.279	0.512827 ± 4	3.7
DLW-8	0.704101 ± 9		0.512758 ± 3	2.3
DYS-2	0.703635 ± 10	0.340	0.512926 ± 4	5.6
DYS-3	0.704268 ± 10	0.280	0.512670 ± 4	0.6
DYS-7	0.704193 ± 8	0.240	0.512695 ± 3	1.1
Harzburgites [$(La/Nd)_n>1$]				
DLW-3	0.703406 ± 8	0.195	0.512966 ± 4	6.4
DLW-4	0.711318 ± 10	0.225	0.512761 ± 4	2.4
DLW-4 (duplicated)	0.711287 ± 10		0.512758 ± 4	2.4
DYS-1	0.703635 ± 8	0.233	0.512713 ± 4	1.5
DYS-6	0.703249 ± 10	0.128	0.512865 ± 4	4.4
DYS-8	0.703241 ± 8	0.141	0.512897 ± 4	5.1
DYS-21	0.703187 ± 9	0.246	0.512927 ± 4	5.6

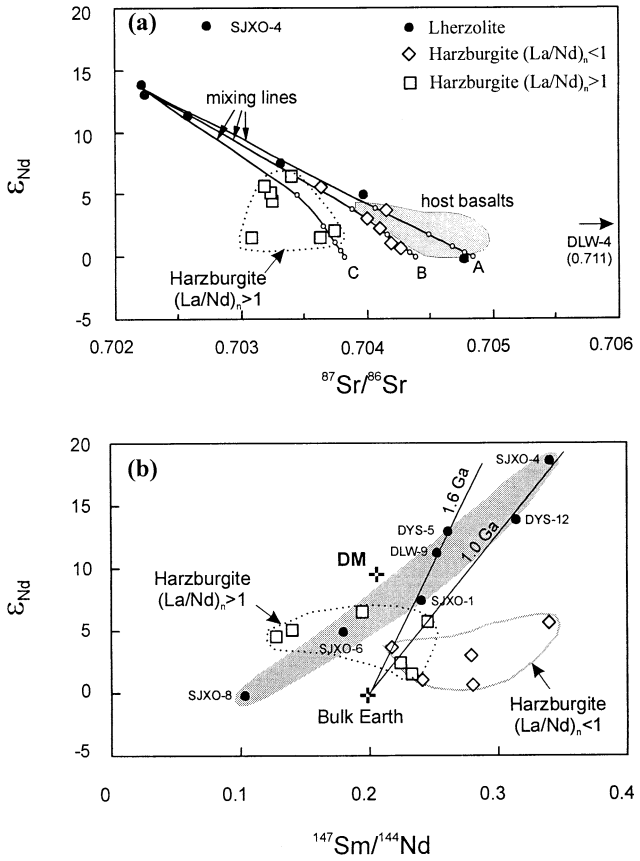

Fig. 7. (a) $^{143}Nd/^{144}Nd$ versus $^{87}Sr/^{86}Sr$ of clinopyroxene separates from the Huinan peridotites. Isotope data of the Cenozoic alkaline basalts (Basu et al., 1991; Liu et al., 1994) from NE China are given for comparison. Published data on Huinan peridotites (Xu et al., 1998c; Fan et al., 2000b) are included in this figure. Mixing lines are between the depleted lherzolite (DYS-12) and component A which is similar to the host basalts, component B (ε_{Nd} = 0; $^{87}Sr/^{86}Sr$=0.70435, Sr = 400 ppm; Nd =28 ppm) and component C (ε_{Nd} = 0; $^{87}Sr/^{86}Sr$=0.7038, Sr = 400 ppm; Nd =20 ppm). (b) ε_{Nd} versus $^{147}Sm/^{144}Nd$ isotopic evolution diagram. The two crosses mark the bulk earth and a model depleted mantle (DM) at ε_{Nd} = 10 evolved from a single stage over the age of the Earth. Sm-Nd ages are calculated with $\lambda = 6.54 \times 10^{-12}$ (yr^{-1}) and the present-day Bulk Earth values are $^{147}Sm/^{144}Nd$ = 0.1967 and $^{143}Nd/^{144}Nd$ = 0.512638.

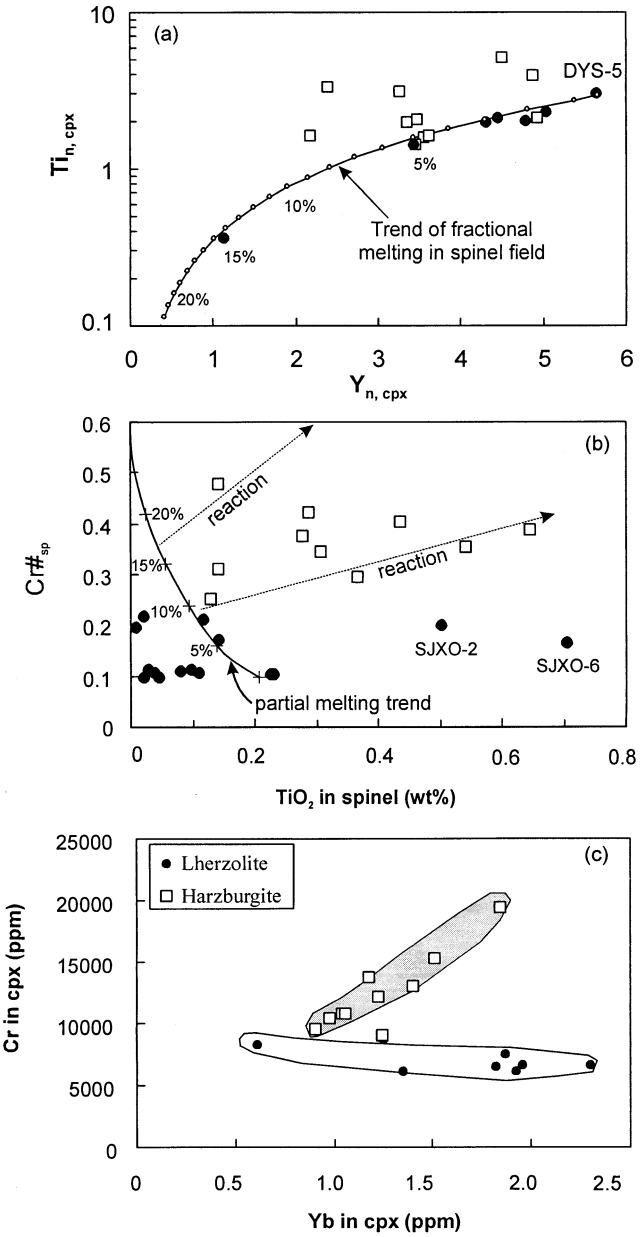

Fig. 8. (a) Ti_n vs. Y_n in clinopyroxene; (b) $Cr\#_{sp}$ vs. TiO_2 in spinel and (c) Cr vs. Yb in clinopyroxene. The trend in (a) is calculated by melting sample DYS-5 using the fractional melting model of Norman et al. (1998). The subscript n in (a) indicates that the Ti and Y concentrations are normalized to primitive mantle (Sun and McDonough, 1989). The partial melting trend (with crosses marking melting degrees) in (b) is modeled by melting a fertile source rock with 0.18 wt.% TiO_2, using the fractional melting equation of Johnson et al. (1990) and the parameters listed by Pearce et al. (2000) except with $Kd_{Ti}^{sp/L}$ being 0.1. The "reaction trends" are those drawn empirically by Pearce et al. (2000) for the Sandwich Forearc peridotites, which were affected by melt-rock reactions.

SJXO-4, the highest ε_{Nd} and relatively higher $^{87}Sr/^{86}Sr$ ratio are attributed to heterogeneity in the lithospheric mantle.

The lithospheric mantle beneath Huinan has locally been affected by cryptic metasomatism. As stated previously, the linear correlation between Sm/Nd and ε_{Nd} (Fig. 7b) may reflect mixing between a depleted mantle source and an enriched component. If this interpretation is correct, it may imply that some lherzolites were affected by cryptic metasomatism, but they retain a LREE/HREE ratio less than the chondritic ratio. This is theoretically possible because metasomatic melts resulting from melt-rock reaction could be either LREE-depleted or LREE-enriched (e.g., Bedini et al., 1997), but it is difficult to evaluate. Metasomatism is more obvious in the cpx-poor lherzolite (i.e., SJXO-8) and in a sample showing signs of Fe-enrichment (i.e., SJXO-6), because these samples show enrichment of highly incompatible elements and Sr-Nd isotopic composition (Fig. 6, Fig. 7). The selective metasomatism in cpx-poor lherzolites may be due to the high connectivity of a melt phase through grain-boundaries in olivine-rich (i.e., cpx-poor) peridotites (Toramaru and Fujii, 1986). The Fe-rich character of SJXO-6 suggests that this sample may be derived from

the vicinity of melt channels. SJXO-6 and SJXO-8 show a trace element pattern characterized by high La/Yb and marked HFSE depletion, somewhat similar to that of carbonate-bearing peridotites (Ionov et al., 1993). However, the negative Sr anomaly in these samples is unexpected for carbonatite melts which show a strong Sr enrichment (Ionov et al., 1993; Ionov, 1998). It has been demonstrated that metasomatic imprints similar to those of carbonate melts may be derived from volatile-rich, small volume silicate melts because of percolation-reaction mechanisms (Bedini et al., 1997). In this event the enriched trace element patterns would correspond to the upper part of a percolation column involving a small melt fraction (Bedini et al., 1997). Given the isotopic similarity between the LREE-enriched lherzolite and the host basalts (Fig. 7a), it is conceivable that the metasomatic agent and host basalts share a common source (cf. mixing line A in Fig. 7a).

5.2. Secondarily Recrystallized Harzburgites: Products of Melt-Rock Reaction?

Although many harzburgites show metasomatic enrichment, their major element chemistry and modal composition are generally considered to be related to extraction of basaltic melts from source regions (Frey and Green, 1974). That is, the metasomatism did not markedly affect the mineralogy but only introduced highly incompatible elements. However, the Huinan harzburgites show some petrographic and geochemical features that are inconsistent with this classic two-stage model.

1. It is noted from Figures 3–4 that most Huinan harzburgites deviate from the common "depletion trend" both in terms of whole rock and mineral compositions. These samples are characterized by relatively higher contents of CaO, Al_2O_3, TiO_2, Na_2O, FeO and incompatible elements (REE and LILE) compared to the depletion trend.
2. Cpx in the Huinan harzburgites has Y and HREE contents significantly higher than in the "residual" harzburgites (Table 3, Fig. 8a, c).
3. A correlation between texture and geochemistry is noted for the peridotites from Huinan. The cpxs in protogranular-porphyroclastic lherzolites show normalized REE patterns, which can be explained by melt extraction and subsequent cryptic metasomatism. In contrast, the cpxs in the harzburgites with secondary recrystallized texture or transitional textures define two groups with quite different normalized REE patterns, either convex upwards with $(La/Nd)_n < 1$ or LREE-enriched with $(La/Nd)_n > 1$ (Fig. 6). In terms of mineralogy and geochemistry, the Huinan harzburgites are comparable to the Boree poikiloblastic xenoliths, which are believed to have formed in the presence of melts and fluids at high melt/rock ratios (Xu et al., 1998a).
4. The plot of $Cr\#_{sp}$ versus TiO_2 content in spinel is particularly effective in distinguishing between partial melting and melt-rock reaction (Pearce et al., 2000). The melting trend in Figure 8b is constructed using the method described by Pearce et al. (2000) except with $Kd_{Ti}^{sp/L} = 0.1$. Modeling shows that TiO_2 contents in spinel in melting residues are generally low (<0.2 wt.%) and the partial melting is monitored by a significant variation in $Cr\#_{sp}$ and a decreasing TiO_2 in spinel (Fig. 8b). Most lherzolite samples (except the Fe-rich SJXO-6 and SJXO-2) from Huinan have relatively low $Cr\#_{sp}$ and Ti contents, and lie close to or below the melting curve (Fig. 8b). In contrast, the harzburgites significantly deviate from the melting curve due to the high-Ti contents in spinel (Fig. 8b). The high Ti content may result from melt-mantle interaction or melt impregnation (Edwards and Malpas, 1996; Xu et al., 1998a). It is noted that the Ti contents in the Huinan harzburgite spinels are comparable to those for the Sandwich Forearc peridotites which have been interpreted as result of melt-rock reactions (Pearce et al., 2000).
5. It is well known that trace element variations during partial melting and cryptic metasomatism are mainly controlled by peridotite/melt partition coefficients (e.g., Navon and Stolper, 1987). Cr is a compatible element in peridotites, whereas REE are incompatible. A negative correlation is thus expected for Cr and REE in residues of partial melting. This is the case for the Huinan lherzolites (Fig. 8c). Cr contents in the Huinan harzburgite cpx are much higher than in lherzolite cpx (Table 3; Fig. 8c). More importantly, Cr is positively correlated with Yb in the harzburgite cpx (Fig. 8c). This indicates a petrogenesis for the Huinan harzburgites other than as residues of partial melting. On the basis of theoretical modeling, Godard et al. (1995) demonstrated that trace elements in peridotites resulting from the melt-rock reaction involving mineralogical change are controlled both by peridotite/melt and intermineral partition coefficients. Consequently, the elements with distinct peridotite/melt partition coefficients but similar intermineral partitioning (e.g., Cr and REE) behave in a similar fashion during melt-rock reaction involving decreasing cpx proportions and production of ol and opx. The positive Cr-Yb correlation in Figure 8c is thus strong evidence that cpx modal variation in the Huinan harzburgites was produced by a melt-rock reaction. Because Cr is concentrated in cpx, reactions, which consume cpx to produce ol+opx, will decrease the size of the cpx reservoir, driving Cr contents higher in remaining cpx.

We thus conclude that the secondary recrystallized harzburgites from Huinan are "reactive" in origin and probably represent products of melt-rock reactions involving cpx dissolution and ol+opx precipitation (e.g., Kelemen et al., 1992, 1998). This mechanism explains the relatively high opx modes in some harzburgites (up to 32%; Table 2), which cannot be generated by partial melting under any temperature and pressure (Walter, 1998). No Zr-Hf anomalies are present in harzburgite cpx. This contrasts with the negative Zr-Hf anomalies in the LREE-enriched lherzolite cpx from Huinan and from other localities in eastern China (Xu et al., 1998b; Fan et al., 2000b). This suggests that the melt responsible for the harzburgite formation is compositionally different from that involved in the cryptic metasomatism in the lherzolites. Ti-enrichment in the harzburgite cpx (Table 3; Fig. 8a) suggests that the percolating melt is basaltic in nature. The convex-upward REE pattern in the harzburgite cpx is diagnostic of equilibrium with LREE-rich melts (e.g., Navon and Stolper, 1987; Bodinier et al., 1988). Compositions of LREE-rich melts in equilibrium with the harzburgite cpx with $(La/Nd)_n < 1$ can be estimated using partition coefficients of Hart and Dunn (1993). The calculated REE patterns of melts (not shown) broadly match

the patterns observed for the host basalts (Liu et al., 1994). A few harzburgites plot between the isotopic composition of LREE-depleted lherzolites and the host basalts (Fig. 7a). However, other harzburgite cpx are plotted left to the field of host basalts (Fig. 7a). Given the similar Sr/Nd ratio between these samples and lherzolites, the melt involved in the formation of the Huinan harzburgites might have an isotopic composition slightly different from those of the host basalts. Figure 7a shows that a simple mixing between the most depleted lherzolites and a component with $^{87}Sr/^{86}Sr$ lightly lower than the host basalts (mixing line B) can nicely account for the isotopic variation of the harzburgite cpx with $(La/Nd)_n < 1$. This suggests that the formation of harzburgites may have proceeded via melt-peridotite reaction at the expense of lherzolites. This melt-rock reaction must have taken place relatively recently because of the lack of a linear correlation between Sm/Nd and ε_{Nd} for the Huinan harzburgites (Fig. 7b).

5.3. Coupled LREE-Enrichment and Low Sr Isotopes in Some Harzburgites

It is interesting to note that the harzburgite cpx with $(La/Nd)_n > 1$ display relatively lower $^{87}Sr/^{86}Sr$ than the harzburgite cpx with $(La/Nd)_n < 1$ at comparable ε_{Nd} (Fig. 7a). This cannot be due to the time effect of radiogenic decay because most harzburgite cpx have a high Sm/Nd and an age correction would yield even lower ε_{Nd}, whereas Sr isotopic ratio remains virtually unchanged given the very low Rb/Sr. The simplest explanation is that the "reactive" harzburgites were metasomatized by an agent, which was much more LREE-enriched than the one inferred for the harzburgites with the convex-upward REE patterns. This agent is relatively depleted in Nb, judging from significant Nb depletion relative to neighboring incompatible elements (Fig. 6f). Metasomatic agents with these characteristics include carbonatitic melt (Ionov et al., 1993), volatile-rich, evolved small melt fractions (Bedini et al., 1997) and H_2O-CO_2 rich fluids. Cpx in some LREE-enriched harzburgites from Huinan have higher Nb contents than in the LREE-depleted samples, indicating the introduction of Nb during metasomatism. This rules out hydrous fluids as the metasomatic agent because experiments have demonstrated a very low solubility of Nb in such fluids (Keppler, 1996). Carbonate and volatile-rich silicate melts are therefore considered as potential metasomatic agents, because they can carry significant amount of trace elements and have low dihedral angle (Watson, 1990). There is no consensus at this stage about the conclusive difference between these different metasomatic styles (e.g., Beccaluva et al., 2001), but the second alternative is preferred because the mineralogical features typical of carbonate metasomatism (e.g., apatite, Yaxley et al., 1998) are not observed at Huinan. The REE patterns of LREE-enriched harzburgites can be understood by chromatographic-type migration of LREE-enriched fluids through LREE-depleted "reactive" harzburgites (Navon and Stolper, 1987; Bodinier et al., 1990). In this metasomatic scheme, elements move through the porous peridotites at rates that are inversely proportional to their solid-melt partition coefficients. The enrichment front of the most incompatible elements moves faster than that of the less incompatible elements. This type of metasomatism produces REE patterns with variable LREE enrichment and unaffected HREE, which are typical of some Huinan harzburgites. Such a process could completely obliterate the initial trace element signature of the harzburgites (i.e., convex-upward REE pattern), as exemplified by DYS-8.

Relatively lower $^{87}Sr/^{86}Sr$ in the harzburgite cpx with $(La/Nd)_n > 1$ compared to those with $(La/Nd)_n < 1$ at comparable ε_{Nd} implies that the $^{87}Sr/^{86}Sr$ ratio of the former (except for DLW-4) was clearly lowered, but the Nd isotopic composition was virtually unchanged during the LREE-enrichment. This suggests that the metasomatic agent is isotopically different than that involved in the formation of "reactive" harzburgites. In this sense, LREE-enrichment may be totally unrelated to the major event responsible for the harzburgite formation. However, it is difficult to understand why this event did not affect lherzolites as well, because the thermometric consideration suggests harzburgite and lherzolites are closely related in space (see next section). As discussed above, the strongly LREE-enriched small melt fractions are expected to be volatile-rich, which would preclude their focusing in refractory peridotites (Bedini et al., 1997).

Alternatively, strongly LREE-enriched small melt fractions may be related to the main harzburgite-forming event, as a result of melt-consuming reaction. Such reaction may occur:

(a) atop the melt-rock reaction column (i.e., atop the harzburgite-forming zone) because of the thermal gradient that existed during the reaction. Lenoir et al. (2001) have demonstrated the existence of this reaction in the Ronda recrystallization front. In this case, the LREE enriched harzburgites would represent a transient stage of the formation of "convex-shaped" harzburgite during lithospheric thermal erosion (Bedini et al., 1997; Xu et al., 1998a);

(b) at a late stage of the reaction process, at the onset of the thermal relaxation that followed the peak of lithospheric thermal erosion, just because of cooling of the peridotite-melt system. This evolution is patent in the whole granular domain of Ronda (Van der Wal and Bodinier, 1996; Garrido and Bodinier, 1999). In this situation, cryptic metasomatic overprints the harzburgite formation but does not record a separate event.

The model (a) can be precluded because it would imply selective isotopic enrichment in Sr if we accept that Sr is more incompatible than Nd in peridotite-melt system. The difference in Sr isotopic ratio between LREE-depleted and LREE-enriched harzburgites can be explained by model (b). This is because the small melt fractions residual after reaction at decreasing melt mass would become more pervasive (Bedini et al., 1997; Xu et al., 1998a) and acquire a more depleted isotopic composition by percolating through lithospheric that were unaffected by the first reaction stage (harzburgite formation). Because of the chromatographic fractionation this depleted character would be transmitted to the LREE-enriched harzburgites for Sr selectively. The proposed chromatographic fractionation of Sr and Nd is consistent with the scatter of the data of the harzburgites with $(La/Nd)_n > 1$ (Fig. 7a) which cannot be easily explained by simple mixing between depleted lherzolites and melts with high Sr/Nd ratios (cf., mixing line C).

While the LREE-enrichment observed in some harzburgites was likely related to the main stage of formation of "reactive" harzburgites, evidence exists for a distinct metasomatic event.

The $^{87}Sr/^{86}Sr$ ratio as high as 0.711 observed for DLW-4 cannot result from time-integrated radiogenic decay given the low Rb/Sr ratio in DLW-4 cpx, nor isotopic exchange between residual melt after reaction and depleted lithospheric mantle as proposed in the model (b). Metasomatism associated with DLW-4 was therefore not related to the formation of "reactive" harzburgites. The extremely high $^{87}Sr/^{86}Sr$ and moderately low ε_{Nd} is reminiscent of an EM2 end-member which was probably derived from slab-subduction (sediment + oceanic crust) (Zindler and Hart, 1986). Identification of EM2-like components in the subcontinental lithosphere mantle beneath eastern China is consistent with previous studies on the basalts and included xenoliths (Basu et al., 1991; Tatsumoto et al., 1992), although the exact origin of this component remains poorly constrained.

5.4. Geodynamic Implications

Secondary recrystallized texture was initially interpreted as a result of annealing and grain growth of equigranular peridotites (Mercier and Nicolas, 1975). However, the data presented in this study confirm the contention (Downes et al., 1992; Van der Wal and Bodinier, 1996; Xu et al., 1998a; Lenoir et al., 2001) that the development of this texture is not an isochemical process and is most likely assisted by the presence of melts. The melt percolation-reaction, which resulted in the petrologic transformation from lherzolite to harzburgite, would ensure wetting of the grain boundaries. This enhances grain boundary diffusion kinetics giving rise to the formation of the recrystallized texture so typical of the Huinan harzburgites. Such a positive correlation between melt/rock ratio and degree of recrystallization is reminiscent of the Ronda orogenic peridotite massif, Spain (Van der Wal and Bodinier 1996), and spinel-facies peridotite xenoliths from the Massif Central, France (Xu et al., 1998a). Inspired by these studies, the petrogenesis of the lherzolites and harzburgites from Huinan can be reconciled within a percolation-reaction column, with different xenolith types corresponding to distinct levels in the column. As discussed above, the Huinan lherzolites may represent samples from the lithosphere mantle where porosity is low and chromatographic metasomatism occurred involving percolation of a small melt fraction. In contrast, the harzburgites may come from the melt-rock reaction zone where porosity is high and basaltic melts have accumulated. This reaction zone is likely to be located within the lithosphere-asthenosphere boundary where thermo-chemical erosion of the lithosphere by upwelling asthenosphere took place.

The development of the peculiar recrystallized texture is commonly associated with a heating event (Xu et al., 1998a; Lenoir et al., 2001). For instance, the granular lherzolites from Boree have equilibrium temperatures (1000 °C) significantly lower than the coarse poikiloblastic harzburgites (>1200 °C, Xu et al., 1998a). However this is not so in the Huinan case, as geothermometry yields similar equilibrium temperatures for the lherzolites and harzburgites. Ambiguity remains as to the spatial relationship between the spinel peridotites with different textural facies, because accurate estimates of equilibrium pressures for spinel facies peridotites is hampered due to a general lack of reliable geobarometer. Currently, the observed temperature variation is believed to reflect a variation in depth of xenolith residence, with an assumption that xenoliths were equilibrated on the same conductive geotherm (e.g., O'Reilly and Griffin, 1996). In this sense, the lherzolites and harzburgites from Huinan may be derived from similar depths. This is not consistent with the above-mentioned inference that the lherzolites and harzburgites correspond to different levels in a percolation-reaction column. The recent thermometric study of the Ronda peridotites (Lenoir et al., 2001) provides clues in understanding this paradox. In Ronda, the deformed peridotites (~ 1050 °C) and the granular peridotites (1200 °C) are separated by a recrystallization front (200 m wide) (Van der Wal and Bodinier, 1996). A similar scenario can be applied to the Huinan case where the lherzolites and harzburgites were indeed closely related but separated in space. Figure 9 offers a possible interpretation of the petrological, thermal and chemical features observed in the harzburgites and lherzolites. Such a location at the base of the lithosphere means that we are in a transition zone between the conductively cooling lithosphere (i.e., mechanical boundary layer) and the convectively cooling asthenosphere.

The different temperature record observed in the Boree-Ronda and Huinan peridotites may be related to the time that has elapsed between thermal events (i.e., lithospheric erosion), entrainment by the host basalts (Boree-Huinan) or tectonic emplacement (Ronda). An active plume has been seismically detected beneath the Massif Central (Granet et al., 1995) and a young mantle diapir is also inferred on the basis of textural data (Nicolas et al., 1987). The development of the Boree harzburgites may be coeval with this recent thermal event (Xu et al., 1998a). In the case of Ronda, the thermal event associated with the development of the recrystallization front occurred in the late geodynamic evolution of Ronda and was aborted by the final emplacement of the massif into the crust along an extension detachment (Lenoir et al., 2001). The short time interval between the thermal event and final entrainment and/or emplacement led to the preservation of a high temperature record in coarse peridotites in both Boree and Ronda cases. The suggestion of thermo-tectonic destruction of the lithospheric root beneath eastern China (e.g., Menzies et al., 1993; Griffin et al., 1998; Gao et al., 2002) is now well founded. This provides an appropriate geodynamic setting for the scenario depicted in Figure 9. In a recent review, Xu (2001) suggested that lithospheric replacement occurred in the late Cretaceous. If the Huinan harzburgites formed by melt-rock interaction at the expense of lithospheric mantle during this thermo-tectonic event, considerable time has elapsed before entrainment during the Quaternary. The relatively long time span between melt-mantle reaction and entrainment is consistent with chemical equilibrium between the constituent minerals in the harzburgites. This ensures that the harzburgites re-equilibrated along the local geothermal gradient as a consequence of thermal decay (Menzies and Xu, 1998).

The above interpretation has two implications:

1. The coarse recrystallized harzburgites might have formed under special conditions where the asthenosphere-derived melt flux and thermal supply were relatively important. These rocks most likely record information about petrologic, geochemical and rheologic changes during lithospheric erosion by upwelling asthenosphere. Coupled chemical and thermo-mechanical erosion (Davies, 1994; Bedini

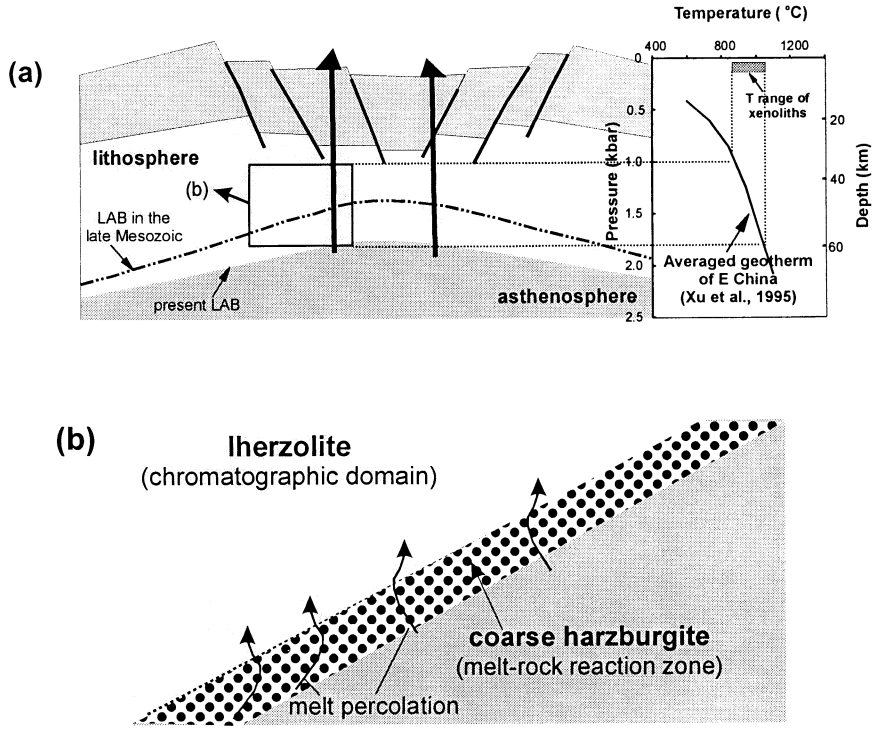

Fig. 9. Schematic illustrations of possible geometric relationships between lherzolites and coarse harzburgites at Huinan. The averaged xenolith-derived geotherm of the lithosphere mantle beneath east China is after Xu et al. (1995). Note the lowering of the lithosphere-asthenosphere boundary (LAB) from the late Mesozoic to present, due to thermal relaxation (Menzies and Xu, 1998).

et al., 1997; Lenoir et al., 2001) is widely considered as an important mechanism to thin the lithosphere. Thermal erosion of the lithosphere is likely to be accompanied by pervasive and reactive flow of asthenospheric melts, which obliterate the initial texture, mineralogy and geochemical signature of the mantle. This process induces weakening of the lithospheric mantle and favors its removal by mantle convection.

2. Although it is widely accepted that the lithospheric mantle beneath eastern China has been significantly thinned as a result of upwelling asthenosphere, uncertainty remains as to the extent of replacement of old lithosphere mantle by "oceanic" peridotites (e.g., Fan et al., 2000b). The xenoliths from Huinan encompass samples from the conductively cooled part of the lithospheric mantle and from the zone where lithospheric erosion by the asthenosphere took place. This strongly indicates a partial replacement of the old lithosphere (Menzies and Xu, 1998). The lithosphere mantle beneath eastern China is likely hybridized with old lithosphere at the uppermost part and newly created "oceanic" type lithosphere in the lower part (e.g., Menzies et al., 1993; Griffin et al., 1998; Fan et al., 2000b; Xu, 2001). However to what extent the "old" lithosphere is an Archaean relic or Phanerozoic in age is not known.

6. SUMMARY AND CONCLUSIONS

The Huinan lherzolites are texturally and compositionally similar to the Group I peridotites from elsewhere. They are samples of the lithospheric mantle that were isolated for 1.0 to 1.6 Ga. The Huinan harzburgites are characterized by a secondary recrystallized texture and distinct geochemical compositions (i.e., convex-upward REE pattern, anomalously high MREE-HREE concentration and positive correlation between Cr-Yb). They resemble the coarse granular xenoliths from southern Massif Central (Lenoir et al., 2000) in terms of texture and equilibrium temperature and are comparable to the Boree poikiloblastic xenoliths (Xu et al., 1998a) with regard to mineralogy and geochemistry. Therefore, the Huinan harzburgites are not simple residues of partial melting but may have resulted from basaltic melt-rock interaction at the expense of the lherzolite protolith. These "reactive" harzburgites were eventually metasomatized by compositionally distinct small volume volatile-rich melts, which may be derived from the main harzburgite-forming event as a result of melt-consuming reaction.

Inspired from the studies on the peridotites from Boree and the Ronda Massif, the petrogenesis of the Huinan lherzolites and harzburgites are reconciled with a percolation-reaction column, with xenoliths of different textures corresponding to distinct levels in the column. While the lherzolites are from the low-porosity domain, the harzburgites are from within the porous reactive zone and are likely to have been produced during erosion of the base of the lithosphere by upwelling melts from the asthenosphere. The absence of a temperature contrast between the Huinan lherzolites and harzburgites suggests a relatively long time in-

terval between lithospheric thinning and eruption of the host basalts. This is consistent with the independent studies that suggest the lithospheric thinning in eastern China was accomplished at the end of the late Cretaceous.

Acknowledgments—We thank B. Orberger and J.-F. Yang for help in the field, Z. Qian, X. Tu, C. Roberts and R. Coyne for technical assistance with analyses. Drs. J.-L. Bodinier, H.-G. Stosch and F.A. Frey are thanked for their thoughtful and constructive reviews which substantially improved the paper. Financial support from the National Science Foundation of China (49925308; 49703042) and from the joint program between the Chinese Academy of Sciences and the Royal Society of London (YGX-MM) is gratefully acknowledged.

Associate editor: F. A. Frey

REFERENCES

Alard O., Bodinier J.-L., Lenoir X., and Dautria J.-M. (1998) Uranium enrichment in the lithospheric mantle: cease studies from Massif Central. *Mineral. Mag.* **62A,** 31–32.

Basu A. R., Wang J. W., Huang W. K., Xie G. H., and Tatsumoto M. (1991) Major element, REE and Pb, Nd and Sr isotopic geochemistry of Cenozoic volcanic rocks of eastern China: implications for origin from suboceanic-type mantle reservoirs. *Earth Planet. Sci. Lett.* **105,** 149–169.

Beccaluva L., Bonadiman C., Coltorti M., Salvini L., and Siena F. (2001) Depletion events, nature of metasomatizing agent and timing of enrichment processes in lithospheric mantle xenoliths from the Veneto volcanic province. *J. Petrol.* **42,** 173–188.

Bedini R. M., Bodinier J.-L., Dautria J. M., and Morten L. (1997) Evolution of LILE-enriched small melt fractions in the lithospheric mantle: a case study from the Easter African Rift. *Earth Planet. Sci. Lett.* **153,** 67–83.

Berger E. T. (1978) Origine cumulatique des enclaves de peridotites a structure poecilitique et tabulaire a gros grains, comparaison avec les tectonites. Consequences sur l'interprrtation de la structure du manteau superieur, ses relations avec la croute inferieure et l'origine des basaltes alcalins. *Bull. Mineral.* **101,** 506–514.

Bodinier J.-L., Dupuy C., and Dostal J. (1988) Geochemistry and petrogenesis of eastern Pyrenean peridotites. *Geochim. Cosmochim. Acta* **52,** 2893–2907.

Bodinier J.-L., Vasseur G., Vernieres J., Dupuy C., and Fabries J. (1990) Mechanisms of mantle metasomatism: geochemical evidence from the Lherz orogenic peridotite. *J. Petrol.* **31,** 597–628.

Brey G. P. and Kohler T. (1990) Geothermobarometry in four-phase lherzolites II. New thermobarometers, and practical assessment of existing thermobarometers. *J. Petrol.* **31,** 1353–1378.

Chen G. Y., Song Z. H., An C. Q., Cheng L. H., Zhuang Z., Fu Z. W., Lu Z. L., and Hu J. F. (1991) Three dimensional crust and upper mantle structure of the North China region (in Chinese with English Abstract). *Acta Geophys. Sinica* **34,** 172–181.

Cohen R. S., O'Nions R. K., and Dawson J. B. (1984) Isotope geochemistry of xenoliths from East Africa: Implications for development of mantle reservoirs and their interaction. *Earth Planet. Sci. Lett.* **68,** 209–220.

Davies G. (1994) Thermomechanical erosion of the lithosphere by mantle plume. *J. Geophys. Res.* **99,** 15709–15722.

Dick J. B. and Bullen T. (1984) Chromian spinel as a petrogenetic indicator in abyssal and alpine-type peridotites and spatially associated lavas. *Contrib. Mineral. Petrol.* **86,** 54–76.

Downes H., Embey-Isztin A., and Thirlwall M. F. (1992) Petrology and geochemistry of spinel peridotite xenoliths from the western Pannonian Basin (Hungary): evidence for an association between enrichment and texture in the upper mantle. *Contrib. Mineral. Petrol.* **109,** 340–354.

Edwards S. J. and Malpas J. (1996) Melt-peridotite interactions in shallow mantle at the East Pacific Rise: evidence from ODP site 895 (Hess Deep). *Mineral. Mag.* **60,** 191–206.

Fan Q. C., Sui J., Liu R., Wei H., and Li N. (2000a) Petrology and geochemistry of Jinlongdingzi active volcano –the most recent basaltic explosive volcano at Longgang. *Chi. J. Geochem.* **19,** 312–317.

Fan W. M., Zhang H. F., Baker J., Javis K. E., Mason P. R. D., and Menzies M. A. (2000b) On and off the North China craton: where is the Archaean keel? *J. Petrol.* **41,** 933–950.

Frey F. A. and Green D. H. (1974) The mineralogy, geochemistry and origin of lherzolite inclusions in Victorian basanites. *Geochim. Cosmochim. Acta* **38,** 1023–1059.

Frey F. A. and Prinz M. (1978) Ultramafic inclusions from San Carlos, Arizona: petrologic and geochemical data bearing on their petrogenesis. *Earth Planet. Sci. Lett.* **38,** 129–176.

Frey F. A., Suen C. J., and Stockman H. W. (1985) The Ronda high temperature peridotite: geochemistry and petrogenesis. *Geochim. Cosmochim. Acta* **49,** 2469–2491.

Galer S. J. G. and O'Nions R. K. (1989) Chemical and isotopic studies of ultramafic inclusions from the San Carlos volcanic field, Arizona: a bearing on their petrogenesis. *J. Petrol.* **30,** 1033–1064.

Gao S., Rudnick R. L., and Carlson R. W. (2002) Re-Os evidence for replacement of ancient mantle lithosphere beneath the North China Craton. *Earth Planet. Sci. Lett.* **198,** 307–322.

Garrido C. J. and Bodinier J. L. (1999) Diversity of mafic rocks in the Ronda peridotite: evidence for pervasive melt- rock reaction during heating of subcontinental lithosphere by upwelling asthenosphere. *J. Petrol.* **40,** 729–754.

Godard M., Bodinier J.-L., and Vasseur G. (1995) Effects of mineralogical reaction on trace element redistributions in mantle rocks during percolation processes: A chromatographic approach. *Earth Planet. Sci. Lett.* **133,** 449–461.

Granet M., Wilson M., and Achauer U. (1995) Imaging a mantle beneath the French Massif Central. *Earth Planet. Sci. Lett.* **136,** 281–296.

Griffin W. L., Zhang A. D., O'Reilly S. Y. and Ryan G. (1998) Phanerozoic evolution of the lithosphere beneath the Sino-Korean Craton. In *Mantle Dynamics and Plate Interactions in East Asia* (eds. M. Flower, S. L. Chung, C. H. Lo and T.Y. Lee), pp. 107–126. Am. Geophys. Union.

Hart S. R. and Dunn T. (1993) Experimental cpx/melt partitioning of 24 trace elements. *Contrib. Mineral. Petrol.* **113,** 1–8.

Hart S. R. and Zindler A. (1986) In search of a bulk Earth composition. *Chem. Geol.* **57,** 247–267.

Hawkesworth C. J., Erlank A. J., Kempton P. D., and Waters F. G. (1990) Mantle metasomatism: isotope and trace element trends in xenoliths from Kimberley, South Africa. *Chem. Geol.* **85,** 19–14.

Ionov D. A. (1998) Trace element composition of mantle-derived carbonates and coexisting phases in peridotite xenoliths from alkali basalts. *J. Petrol.* **39,** 1931–1942.

Ionov D. A., Dupuy C., O'Reilly S. Y., Kopylova M. G., and Genshaft Y. S. (1993) Carbonated peridotite xenoliths from Spitsbergen: implications for trace element signature of mantle carbonate metasomatism. *Earth Planet. Sci. Lett.* **119,** 283–297.

Ionov D. A., Kramm U., and Stosch H.-G. (1992) Evolution of the upper mantle beneath the southern Baikal rift zone: an Sr-Nd isotope study of xenoliths from the Bartoy volcanoes. *Contrib. Mineral. Petrol.* **111,** 235–247.

Jagoutz E., Palme H., Baddenhausen H., Blum K., Cendales M., Drebus G., Spettel B., Lorenz V. and Wanke H. (1979) The abundances of major, minor and trace elements in the earth's mantle as derived from primitive ultramafic nodules. *Proc. Lunar Planet. Sci Conf.* **10th,** 1031–2050.

Johnson K. T. M., Dick H. J. B., and Shimizu N. (1990) Melting in the oceanic upper mantle: An ion microprobe study of diopsides in abyssal peridotites. *J. Geophy. Res.* **95,** 2661–2678.

Kelemen P. B., Dick H. J. B., and Quick J. E. (1992) Formation of harzburgite by pervasive melt/rock reaction in the upper mantle. *Nature* **358,** 635–641.

Kelemen P. B., Hart S. R., and Bernstein S. (1998) Silica enrichment in the continental upper mantle via melt/rock reaction. *Earth Planet. Sci. Lett.* **164,** 387–406.

Keppler H. (1996) Constraints from partitioning experiments on the composition of subduction-zone fluids. *Nature* **380,** 237–239.

Lenoir X., Garrido C. J., Bodinier J.-L., and Dautria J.-M. (2000) Contrasting lithospheric mantle domains beneath the Massif Central

(France) revealed by geochemistry of peridotite xenoliths. *Earth Planet. Sci. Lett.* **181,** 359–375.

Lenoir X., Garrido C. J., Bodinier J.-L., Dautria J.-M., and Gervilla F. (2001) The recrystallization front of the Ronda peridotite: evidence for melting and thermal erosion of subcontinental lithospheric mantle beneath the Alboran Basin. *J. Petrol.* **42,** 141–158.

Liu C. Q., Masuda A., and Xie G. H. (1994) Major- and trace-element compositions of Cenozoic basalts in eastern China: petrogenesis and mantle source. *Chem. Geol.* **114,** 19–42.

Liu R. X., Chen W. J., Sun J. Z., and Li D. M. (1992) The K-Ar age and tectonic environment of Cenozoic volcanic rock in China. In *The age and geochemistry of Cenozoic volcanic rock in China* (ed. R. X. Liu) pp. 1–43. Seismologic Press (in Chinese).

McDonough W. F. and Frey F. A. (1989) Rare earth elements in upper mantle rocks. In *Geochemistry and mineralogy of rare earth elements* (eds. B. Lipin and G. McKay), *Rev. Mineral.* **21,** 99–145.

McDonough W. F. and McCulloch M. T. (1987) The southeast Australian lithospheric mantle: isotopic and geochemical constrains on its growth and evolution. *Earth Planet. Sci. Lett.* **86,** 327–340.

Menzies M. A., Fan W. M., and Zhang M. (1993) Palaeozoic and Cenozoic lithoprobes and the loss of > 120 km of Archaean lithosphere, Sino-Korean craton, China. In *Magmatic processes and plate tectonics* (eds. H. M. Prichard, T. Alabaster, N. B. W. Harris and V. R. Neary), *Geol. Soc. Spel. Pub.* **76,** 71–78.

Menzies M. A., Kempton P. D., and Dungan M. (1985) Interaction of continental lithosphere and asthenospheric melts below the Geronimo Volcanic Field, Arizona, U.S.A. *J. Petrol.* **26,** 663–693.

Menzies M. A. and Murthy V. R. (1980) Enriched mantle: Nd and Sr isotopes in diopsides from kimberlite nodules. *Nature* **283,** 634–636.

Menzies M. A. and Halliday A. (1988) Lithospheric mantle domains beneath the Archean and Proterozoic crust of Scotland. *J. Petrol.* **Special Lithosphere Issue,** 275–302.

Menzies M. A. and Xu Y. G. (1998) Geodynamics of the North China Craton. In *Mantle Dynamics and Plate Interactions in East Asia* (eds. M. Flower, S. L. Chung, C. H. Lo and T.Y. Lee), pp. 155–165. Am. Geophys. Union.

Mercier J.-C. C. and Nicolas A. (1975) Textures and fabrics of upper mantle peridotites as illustrated by xenoliths from basalts. *J. Petrol.* **16,** 454–487.

Navon O. and Stolper E. (1987) Geochemical consequence of melt percolation: the upper mantle as a chromatographic column. *J. Geol.* **95,** 285–307.

Nicolas A., Lucazeau F. and Bayer R. (1987) Peridotite xenoliths in Massif Central basalts: textural and geophysical evidence for asthenospheric diapirism. In *Mantle xenoliths* (ed. P. H. Nixon), pp. 563–574. John Wiley & Sons Ltd.

Niu Y. (1997) Mantle melting and melt exaction processes beneath ocean ridges: evidence from abyssal peridotites. *J. Petrol.* **38,** 1047–1074.

Norman M. D. (1998) Melting and metasomatism in the continental lithosphere: laser ablation ICPMS analysis of minerals in spinel lherzolites from eastern Australia. *Contrib. Mineral. Petrol.* **130,** 240–255.

O'Reilly S. Y. and Griffin W. L. (1996) 4-D lithosphere mapping: methodology and examples. *Tectonophysics* **262,** 3–18.

Pearce J. A., Barker P. F., Edwards S. J., Parkinson I. J., and Leat P. T. (2000) Geochemistry and tectonic significance of peridotites from the South Sandwich arc-basin system, South Atlantic. *Contrib. Mineral. Petrol.* **139,** 36–53.

Roden M. F., Irving A. J., and Murthy V. R. (1988) Isotopic and trace element composition of the upper mantle beneath a young continental rift: results from Kilbourne Hole, New Mexico. *Geochim. Cosmochim. Acta* **52,** 461–473.

Shi L., Francis D., Ludden J., Frederiksen A., and Bostock M. (1998) Xenolith evidence for lithospheric melting above anomalously hot mantle under the northern Canadian Cordillera. *Contrib. Mineral. Petrol.* **131,** 39–53.

Stosch H. G. and Lugmair G. W. (1986) Trace elements and Sr and Nd isotope geochemistry of peridotite xenoliths from the Eifel (W. Germany) and their bearing on the evolution of the subcontinental lithosphere? *Earth Planet. Sci. Lett.* **80,** 281–298.

Stosch H. G., Lugmair G. W., and Kovalenko V. I. (1986) Spinel peridotite xenoliths from the Tariat Depression, Mongolia. II: Geochemistry and Nd and Sr isotopic composition and their implication for the evolution of the sub-continental lithosphere. *Geochim. Cosmochim. Acta* **50,** 2601–2614.

Sun S.-S. and McDonough W. F. (1989) Chemical and isotopic systematics of oceanic basalts: implications for mantle composition and processes. In *Magmatism in the Ocean Basins* (eds. A. D. Saunders and M. J. Norry), *Geol. Soc. Spel. Pub.* **42,** 313–345.

Takazawa E., Frey F. A., Shimizu N., and Obata M. (2000) Whole rock compositional variation in an upper mantle peridotite (Horoman, Hokkaido, Japan): Are they consistent with a partial melting process? *Geochim. Cosmochim. Acta* **64,** 695–716.

Tatsumoto M., Basu A. R., Huang W. K., Wang J. W., and Xie G. H. (1992) Sr, Nd, and Pb isotopes of ultramafic xenoliths in volcanic rocks of Eastern China: enriched components EMI and EMII in subcontinental lithosphere. *Earth Planet. Sci. Lett.* **113,** 107–128.

Thirlwall M. F. (1991) Long-term reproducibility of multicollector Sr and Nd isotope ratio analysis. *Chem. Geol.* **94,** 85–104.

Toramaru A. and Fujii N. (1986) Connectivity of melt phase in a partially molten peridotite. *J. Geophy. Res.* **91,** 9239–9252.

Walter M. J. (1998) Melting of garnet peridotite and the origin of komatiite and depleted lithosphere. *J. Petrol.* **39,** 29–60.

Watson E. B., Brenan J. M., and Baker D. B. (1990) Distribution of fluids in the continental mantle. In *Continental mantle* (ed. M. A. Menzies), pp. 111–125. Oxford Science Publication.

Witt-Eickschen G. E. and Seck H. A. (1991) Solubility of Ca and Al in orthopyroxene from spinel peridotite: an improved version of an empirical geothermometer. *Contrib. Mineral. Petrol.* **106,** 431–439.

Van der Wal D. and Bodinier J.-L. (1996) Origin of the recrystallisation front in the Ronda peridotite by km-scale pervasive porous melts flow. *Contrib. Mineral. Petrol.* **122,** 387–405.

Xu S., Nagao K., Uto KWakita H., Nakai S., and Liu C. (1998c) He, Sr and Nd isotopes of mantle-derived xenoliths in volcanic rocks in NE China. *J. Southeast Asian Earth Sci.* **16,** 547–556.

Xu Y. G. (2001) Thermo-tectonic destruction of the Archaean lithospheric keel beneath eastern China: evidence, timing and mechanism. *Physics and Chemistry of the Earth (A).* **26,** 747–757.

Xu Y. G. (2002) Evidence for crustal components in mantle source and constraints on recycling mechanism: pyroxenite xenoliths from Hannuoba, North China. *Chem. Geol.* **182,** 301–322.

Xu Y. G., Lin C. Y., Shi L. B., Mercier J.-C. C., and Ross J. V. (1995) Upper mantle geotherm for eastern China and its geological implications. *Science in China (Series B).* **38,** 1482–1492.

Xu Y. G., Menzies M. A., Bodinier J.-L., Bedini R. M., Vroon P., and Mercier J.-C. (1998a) Melt percolation-reaction atop the plume: evidence from poikiloblastic spinel harzburgite xenoliths from Boree (Massif Central, France). *Contrib. Mineral. Petrol.* **132,** 65–84.

Xu Y. G., Menzies M. A., Vroon P., Mercier J.-C., and Lin C. Y. (1998b) Texture-temperature-geochemistry relationships in the upper mantle as revealed from spinel peridotite xenoliths from Wangqing, NE China. *J. Petrol.* **39,** 469–493.

Yaxley G. M., Green D. H., and Kamenetsky V. (1998) Carbonatite metasomatism in the southeastern Australian lithosphere. *J. Petrol.* **39,** 1917–1930.

Zindler A. and Hart S. R. (1986) Chemical geodynamics. *Ann. Rev. Earth Planet. Sci.* **14,** 493–571.